VILNIUS UNIVERSITY
FACULTY OF MATHEMATICS AND INFORMATICS
MODELLING AND DATA ANALYSIS MASTER'S STUDY PROGRAMME

Master's Thesis

Comparative analysis of similarity measures for multidimensional streaming data

Daugiamačių srautinių duomenų panašumo matų lyginamoji analizė

Maksym Ponomarenko

Supervisor: dr. Viktor Medvedev

Vilnius, 2021

Contents

Abstract **4**

Introduction **6**

Theoretical part **9**

Research relevance 9

Artificial intelligence in HealthcareSurvey Report 9

Big Data Analytics in Healthcare 10

Literature review 13

Time series data 13

Similarity measures techniques 13

Euclidean Distance 14

Manhattan Distance 15

Maximum Distance 15

Minkowski Distance 15

Frobenius norm 15

Dynamic time warping: 15

Longest Common SubSequence: 18

Principal Component Analysis (PCA) similarity factor 19

Convolutional neural network: 19

Weights and Basis 20

The ReLU layer 20

Back-Propagation Algorithm 21

Autoencoder 21

Biosensors 22

Photoplethysmography (PPG) 24

Electrocardiogram (ECG) 25

Modern sensors capabilities 27

Conclusions 27

Experimental results **29**

Data 29

Data preparation 32

Exploratory data analysis 36

The Anomaly detection Framework structure 37

Models 38

The Similarity measure model 38

The Autoencoder model 40

Anomaly detection framework 43

Conclusions **44**

References **45**

Appendix 1 (Autoencoder architecture) **51**

Abstract

This work is focused on the analysis of multivariate time series using a similarity measure in various fields. The aim of this work is to provide a robust framework for multidimensional signal analysis. The purpose of this framework should be cardiac anomaly detection via ECG (Electrocardiogram) using PPG (Photoplethysmogram) as an additional source of information via multidimensional streaming time series anomaly detection algorithms and deep learning algorithms. Some limitations have been made in order to make this framework applicable to modern tasks and implementable for wearable devices, such as computational complexity and choice of physiological signals that is realistic to acquire using wearable sensors. The key mathematical algorithms of this framework were implemented. The author managed to create a framework that is illustrated in *Figure 25*. This solution uses the combination of three methods: Data mining to extract cardiac cycle-like segments, Similarity similarity measure model for pre-filtering on extracted segments and Convolutional Autoencoder in order to perform more advanced anomaly detection on data that has been received after the previous model. The combination of these techniques allows to increase both detection speed, accuracy and flexibility in terms of regulatable abnormality measure threshold that can be adjusted .

Keywords: multivariate time series, similarity measure, streaming data, deep learning, autoencoders, similarity measure, biosensor, anomaly detection, wearable sensors

Santrauka

Šiame darbe analizuojamos daugiamatės laiko eilučių panašumo matai. Šio darbo tikslas - pateikti patikimą daugiamačių srautnių duomenų analizės sistemą. Šios sistemos paskirtis turėtų būti širdies anomalijų aptikimas naudojant EKG (elektrokardiogramą), naudojant PPG (fotopletizmogramą) kaip papildomą informacijos šaltinį, taikant daugiamačių srautinių duomenų anomalijų aptikimo algoritmus ir gilaus mokymosi algoritmus. Siekiant, kad ši sistema būtų pritaikoma šiuolaikinėms užduotims ir įgyvendinama nešiojamuosiuose įrenginiuose, buvo nustatyti tam tikri apribojimai, pavyzdžiui, skaičiavimo sudėtingumas ir fiziologinių signalų, kuriuos realu gauti naudojant nešiojamuosius jutiklius, pasirinkimas. Buvo įgyvendinti pagrindiniai šios sistemos matematiniai algoritmai. Autoriui pavyko sukurti sistemą, kuri pavaizduota 1 pav. Šiame sprendime naudojamas trijų metodų derinys: duomenų tyrybos metodai, siekiant išskirti į širdies ciklą panašius segmentus, panašumo matų modelis išskirtiems segmentams filtruoti ir autoenkoderio tipo konvoliucinis neuroninis tinklas, kad būtų galima atlikti pažangesnį anomalijų aptikimą duomenyse, gautuose po ankstesnio modelio. Šių metodų derinys leidžia padidinti anomalijų aptikimo greitį, tikslumą ir lankstumą reguliuojamo anomalijų matavimo slenksčio, kurį galima reguliuoti, požiūriu.

Raktiniai žodžiai: daugiamatės laiko eilutės, panašumo matas, srauto duomenys, gilusis mokymasis, autoenkoderio tipo konvoliucinis neuroninis tinklas, biojutiklis, anomalijų aptikimas, dėvimi jutikliai

Introduction

This research presents a framework for multidimensional anomaly detection of anomalies in streaming ECG data. The framework tries to detect anomalies in ECG using PPG as an additional source of information. The whole structure of this framework is described in *Figure 25*. Additional sources such as heart rate (HR), oxygen saturation (SPO2), and pulse transmit time (PTT) also can be used as an additional third stage of filtering 'Classifier' which is not implemented in this research, but this data is realistic to obtain with modern sensors. This solution uses the combination of three methods: Data mining to extract cardiac cycle-like segments, Similarity measure model for pre-filtering on extracted segments and Convolutional Autoencoder in order to perform more advanced anomaly detection on data that has been received after the previous model. The combination of these techniques allows to increase both detection speed, accuracy and flexibility in terms of regulateble abnormality measure threshold that can be adjusted .

To make my framework relevant to real world tasks I had to choose sources of streaming data that are realistic to acquire with wearable biosensors. For this work, the authors chose ECG and PPG time series because this combination of required sensors can be implemented in a single device and can provide a reasonable level of credibility. Both of these physiological signals have a relationship with each other and can be used in combination for anomaly detection in cardiac system [1]. To use this relationship it is critical to understand basics principles of ECG and PPG functioning, PPG waveforms are synchronized with ECG because they both related to blood volume, while using PPG for detection of abnormalities in ECG is critical to look at PPG time series before the time when ECG anomaly occurs. Principles of PPG and ECG functioning that affect the authors' framework are described in the literature review. Also it is important for splitting ECG and PPG into segments for analysis, segments I work with are R-R intervals from ECG and PPG segments that correspond to previous ECG R-R intervals.

The author made a huge effort in investigating modern and prospective applications of signal analysis in the field of healthcare. The Healthcare industry is in the stage of rapid and fundamental changes now. The current situation of biosensors implementation in Healthcare, data analysis applications and the situation in Healthcare market is described in the Relevance section. To prove the author's concept that existing or prospective biosensors can provide required data with appropriate signal accuracy, key biosensor market players have been inspected.[2]. Example of a device that can be used as a prototype to implement such kind of framework. [3]

There are two datasets that have been used, 'MIMIC-III Waveform matched subsets' and 'Combined Measurement of ECG, Breathing and Seismocardiography'[4,5]. It is important to highlight that 'MIMIC-III Waveform matched subsets' contain real-world data. A detailed description of data is given in the Data section below.

In both MIMIC-III Waveform matched subsets and 'Combined Measurement of ECG, Breathing and Seismocardiography' dataset are represented as a continuous time series. 'Combined measurement of ECG, Breathing and Seismocardiography' dataset has been used as train data for autoencoder and 'MIMIC-III Waveform Matched Subsets' dataset to apply

the final model. ‘Combined measurement of ECG, Breathing and Seismocardiography’ dataset includes only presumably healthy patients in normal condition so we can assume that they have normal ECG characteristics. ‘MIMIC-III Waveform Matched Subsets’ dataset have long time series with lots of anomalies, most of them occur because of incorrect sensor usage because some records are more than 50 hours long. I don't want to consider these segments as anomalies so I applied data mining techniques to find cardiac cycles like ECG segments. To detect these segments I used a sliding window approach. Segments I looked for are R-R intervals in ECG and corresponding to this PPG time series segments. To make analysis more simple I extracted R-R intervals from ECG.

Received data segments require pre-processing first. Data segment will be used as an input for all next stages of the framework . All inputs should have the same lengths, so after cutting R-R intervals from time series we have to add zero values to the end of the R-R interval. Then I scaled the time series segment using the Min-Max scaler for intervals from 0 to 1.

The framework is a combination of models which interact with each-other. The structure of the framework is described in the appropriate section, the structure of the whole framework is shown in *Figure 25*.

The key advantage of the Similarity Measure model it is calculation complexity combined with optimization abilities, In this framework use Similarity measure model as first stage of anomaly detection in order to filter mods obvious normal segments, after experimenting with different SImilarity measure techniques, that are described in literature review, I took Dynamic Time Warping algorithm because of his resistance to length variability. Similarity Measure model compares ECG and PPG segments in the way that is described above. After filtering data with SImilarity measure model we obtain both normal and abnormal ECG segments, then based on similarity measure value the author took 5%,1%,0.1% of most abnormal ECG segments for further analysis in the Autoencoder Model.

The Autoencoder uses suspicious ECG segments to reconstruct most similar normal segments and return this segment as output. After reconstruction we can calculate reconstruction error, for segments which are close to normal reconstruction error will be small because they are already alike to normal ECG segments. For abnormal segments reconstruction error will be higher. By analyzing reconstruction errors we can detect abnormal R-R intervals

The aim of this work is to provide a robust multivariate streaming data analysis framework based on various similarity measures for anomaly detection problems**.** The purpose of this framework should be cardiac anomaly detection via ECG (Electrocardiogram) using PPG (Photoplethysmogram) as an additional source of information via multidimensional streaming time series anomaly detection algorithms and deep learning algorithms.

To achieve the proposed aim, five main **tasks** have been identified:

- *Explore the use of similarity measures to analyse multidimensional streaming data.*
- *Identify appropriate methods to develop a solution.*
- *Combine similarity measure methods with deep learning methods.*

- *To make sure that the proposed model is suitable for real-world tasks, choose an appropriate source of streaming data.*
- *Conduct experiments to determine the suitability of the method for anomaly detection.*

Theoretical part

Research relevance

Artificial intelligence in HealthcareSurvey Report

Applications of Artificial Intelligence (AI) in Healthcare present challenges and considerations unique to that industry. They conducted a survey specifically targeted to AI in healthcare to understand more about the current trends and approaches in that space. The insights and trends revealed in this report are informed by the intentional contrast in the survey respondents we targeted: organizations with years of history deploying AI applications in production versus those which are newly exploring AI, Technical Leaders versus general respondents, relative company size, and geographic region.

Respondents from 49 countries have participated in this survey. The survey includes 373 respondents from the healthcare companies which includes Technical leaders and employees from Other IT related roles.

Demographics companies by countries :

- America 54% (US 48%)
- Asia-Pacific 29% (India 23%)
- Europe, Middle East, Africa 16%

Respondents are grouped based on response to a question that measured their company's stage of AI adoption. As we can see from *Figure 1,* 74% of respondents are considering AI implementation in their company.

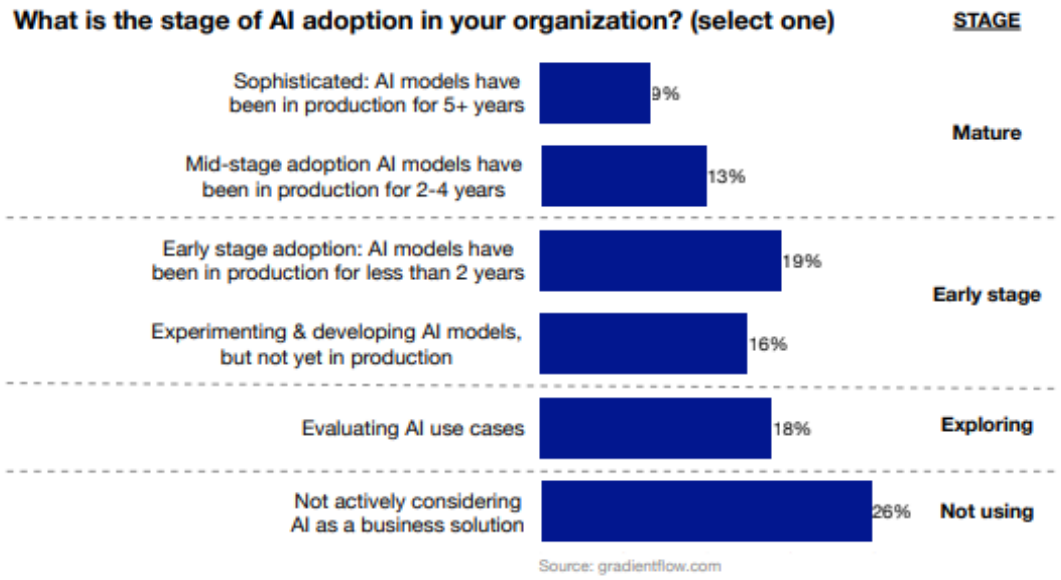

Figure 1 *Answers to questions about the stage of Artificial intelligence adaptation in the respondent's organization.*

Question about software that companies are currently using or plan to invest in until 2021 *(see Figure 2).*

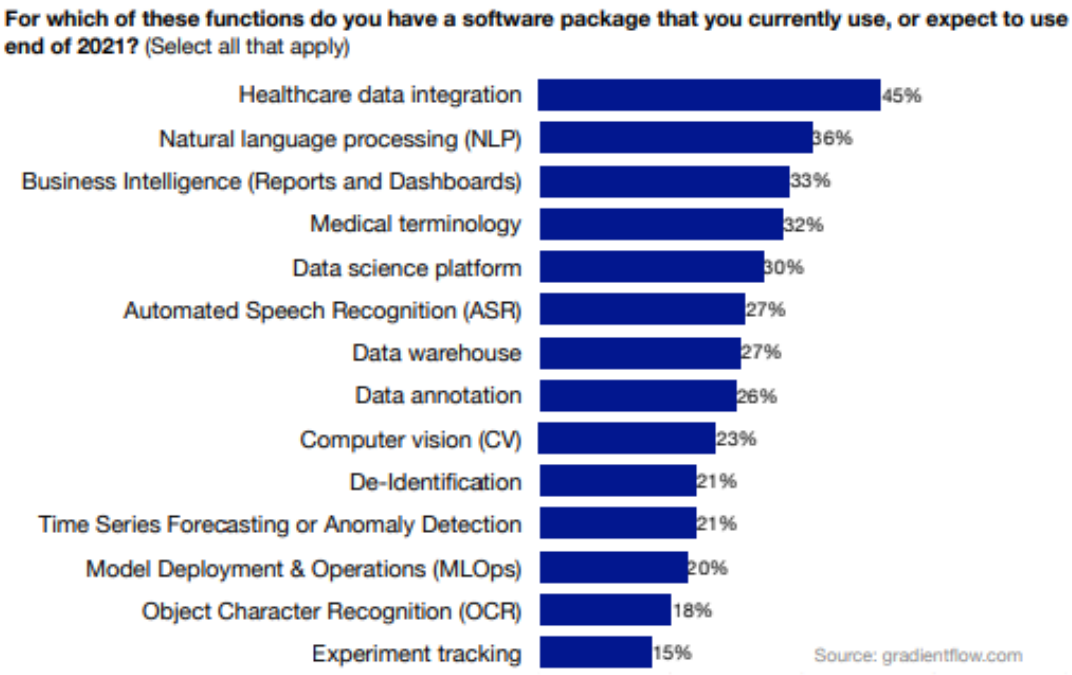

Figure 2 *Answer to question about types of software application that respondents use in their companies.*

We can see that Time Series forecasting or Anomaly detection software holds 21% of all respondents. Question about data type of interest is shown in *Figure 3*.

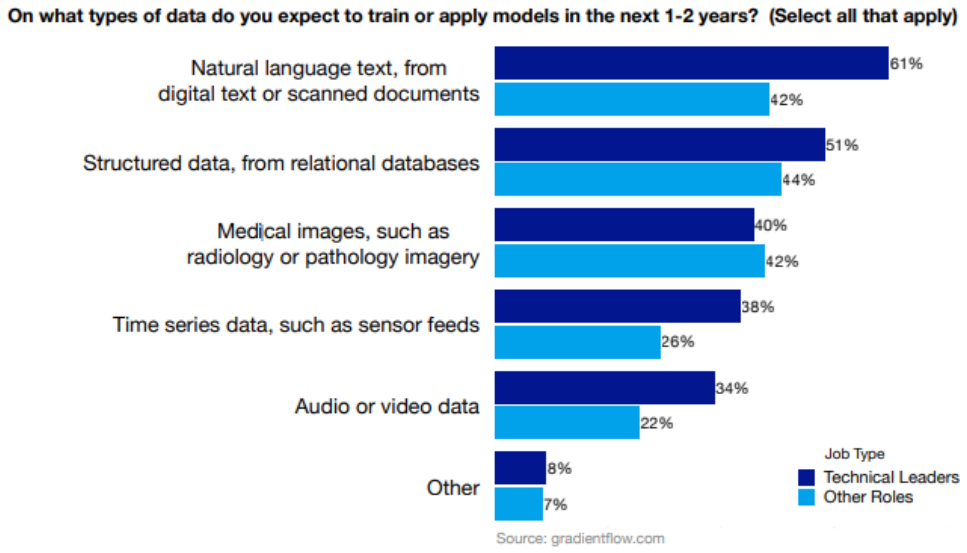

Figure 3*. Answers of respondents about data types of interest.*

Time Series data particularly to sensor feeds holds 38% which is a great result for niche topics like sensor data analysis.

Big Data Analytics in Healthcare

Healthcare systems currently use a number of different continuous monitoring devices that use individual physiological waveforms or discrete vital information to provide alert

mechanisms in the event of an overt event. However, such unreasonable approaches to the design and implementation of alarm systems are generally unreliable, and many of them can cause "anxious fatigue" in both caregivers and patients [10–12]. In this situation, the opportunity to discover new medical knowledge is limited by previous knowledge, which, as a rule, does not allow the maximum use of data from large time series. The reason that these alarm mechanisms tend to fail is primarily because these systems tend to rely on individual sources of information, without having the context of the true physiological state of patients from a broader and more comprehensive point of view. Therefore, there is a need to develop improved and more comprehensive approaches to the study of interactions and correlations between multimodal clinical time series data. This is important because research continues to show that people are reluctant to change, which affects more than two signals. What is very important in our case, because we will use a multidimensional similarity measure analysis approach. This approach is more tolerant to small errors because it outputs a measure of similarity or abnormality in our case and we will use multidimensional streaming inputs that should reduce false alarms.

A huge amount of data in a short period of time is obtained in intensive care units (ICUs), where a large amount of physiological data is obtained from each patient. Thus, the potential for the development of anomaly detection systems in the intensive care unit has been recognized by many researchers. A scalable infrastructure is proposed to develop a patient management system that combines static and flow data tracked from critically ill patients in the intensive care unit for data analysis and warning of medical personnel about critical events in real-time [7]. Similarly, Bressan et al. designed Neonatal Intensive Care Unit, which used streaming data from infusion pumps, EEG monitors, cerebral oxygenation monitors, etc. to support the clinical solution [8]

The combination of multiple waveform information available in the MIMIC III database is used for early detection of cardiovascular instability in patients [119]. This is a set of data that we will use to test the system. Many types of physiological data recorded in operative and preoperative conditions, as well as how the analytical system can use these data to continuously monitor the condition of patients during, after and before surgery, are described in [9].

The development of multimodal monitoring of patients with traumatic brain injury and individual care of patients is considered in [10]. Many researchers investigated whether multimodal brain monitoring using TCD, EEG, and SEP reduces the incidence of serious neurological complications in patients undergoing cardiac surgery. Multimodal brain monitoring has reduced the duration of mechanical ventilation required by patients, as well as being in intensive care and healthcare. The concepts of multimodal monitoring of secondary traumatic brain injury in neurocritical care, as well as outline the initial and future approaches using information tools to understand and apply such data for clinical care are described in [11].

As sophisticated physiological monitoring devices become smaller, cheaper, and more portable, personal monitoring tools are used outside the clinical environment by both patients and enthusiasts. However, like clinical programs, combining information gathered from multiple portable devices can be a challenge at the same time. Pantelopoulos and Burbakis discussed research and development of wearable biosensor systems and identified advantages

and disadvantages in this area of research [12]. Similarly, portable and connected electrocardiograms, devices for measuring blood pressure and body weight are used to create a network study of telemedicine [13]. The variety of fixed as well as mobile sensors available for data in the health sector and the ways in which such data can be used to develop patient care technologies are explored in [14].

There are several key trends and new challenges I want to consider in my work:

1. *Telehealth* is the use of electronic information and telecommunications technologies to support and promote long-distance clinical health care, patient and professional health-related education, public health and health administration. Technologies include videoconferencing, the internet, store-and-forward imaging, streaming media, and terrestrial and wireless communications. "For healthcare professionals, it allows high-risk patients to be monitored and treated more easily, as well as improving efficiency and work-life balance."

2. *Recent developments in wearable biosensors technology and wearable electronics market growth* [2]. Wearable sensors are currently in the stage of rapid development, they are becoming smarter and smaller year by year, this is dictated by leaders in the consumer electronic market which push smart or fitness watchers at higher rates each year. This leads to improvement of sensors (which can be used as biosensors) with almost each new generation of devices.

3. *Telemedicine* popularity is strongly linked to rapid Telehealth implementation into Healthcare systems. Telemedicine is the broad description of providing medical and healthcare services by means of telecommunications [15]. During the Covid-19, US officials have opened access to these remote health services. More people than ever before are speaking to their doctor using video conferencing technology using their home broadband connection.

4. *Health insurance prices growth.* The Healthcare insurance market has grown tremendously during the last 10 years. Telehealth and wearable biosensor implementation can significantly affect insurance prices: [16,17,18].

From paper "50 Ideas to Make Healthcare More Affordable, Accessible and Efficient [30] "author highlighted such ideas :

1. Online doctor appointment scheduling can reduce pressure on physicians due to better management of human resources and lead to cost reduction. Constant lack of human resources is a common problem of the modern healthcare system. This is caused by the constantly growing healthcare services market[20].
2. Better forecasting models and detection of diseases in early stages of development, can be achieved by health monitoring via biosensors. There are multiple devices which able to detect cardiovascular system instability, for example, Apple Watch Series 4 for Arrhythmia Detection [21] , diseases like left bundle branch block (LBBB), right bundle branch block (RBBB), ventricular premature contractions (VPC), and atrial premature contractions (APC) .Or algorithms for ECG or PPG anomaly detection, which can be considered as symptoms of a disease or can be a indicator of cardiovascular instability.

3. Senior people are at higher risk because of their age. But senior people benefit the most from constant sensor monitoring and Telemedicine systems. Monitoring via wearable sensors can require minimal expertise from the side of senior users, also telehealth and online physician consultations can be more convenient for old people. Wearable sensors systems can detect instability of the cardiovascular system. Included accelerometers or external radio sensors can detect if a person fell[22], also the same sensors can be used for detection of abnormal gait [23]or suspicious low activity of the person.

Literature review

Time series data

In this case data is represented as a time-series which can be represented as data in chronological order. The data is obtained over some period. In my case we will use streaming data from the sensors, but this streaming data would be transformed to the finite intervals for further analysis. One of the classic definitions of time-series has been given in the famous journal Spiegel "A time series is a set of observations taken at specified times, usually at equal intervals. In my case this is ECG data.

A time series T is an ordered sequence of n real-valued variables

$$T = (t_1, t_2 ... t_n) \, t_i \in \mathbb{R}$$

We will investigate the multivariate physiological time series. A physiological time series is a series of medical observations. To interact with streaming time series I will cut them in finite pieces during data mining procedures.

Similarity measures techniques

One of the tools of Data Mining in time series mining is the similarity problem. It is a comparison of two time series or segments of time series in order to determine whether they are similar or not. For example, if we want to 'mine' specific signals along a whole time series we can compare segments that we are looking for to supposed segments in full time series. The way we do this is called Similarity measure. Usually, the choice of a similarity measure can affect the result of data mining tasks. Similarity measure we mean a method, which compares two time series and returns the index or value of their similarity. If the input data consist of multiple features Similarity Measure algorithms can be applied to multidimensional time series.

Distance-based Similarity Measure approach is the most popular way of determining similarity between time series. The most important aspects of this method are the choice of appropriate distance or similarity measure. If the distance between two time series is small, it means that they have similarities. Depending how we calculate the distance between time series our algorithm can catch different particle qualities of our data, also there are different ways to calculate the same distances. Performance of the Similarity Measure algorithm is hardly dependent on distance and approach of calculation distances between time series, in a most simple way we calculate distance between the same points of time.

The distance between two time series $Q = (q_q, q_2, \ldots, q_n)$ and $S = (s_1, s_2, \ldots, s_m)$ is defined using a proximity measure - a function that returns the nonnegative distance $d(Q,S)$ between them. A distance metric is a proximity measure that for every time series *Q, S* and *X* satisfies the following conditions:

1. **Reflexivity :** *d(Q,S) = 0* if and only if *Q = S*
2. **Symmetry :** *d(Q,S) = d(S,Q)*
3. **Triangle inequality:** *d(Q,S)*$\leq$*d(Q,S)+d(X,S)*

For convenience in Similarity Measure frequently used scale from 0 to 1.

Converting distance into similarity, and vice versa is possible by means of the following formula [24,25, 26]:

$$sim(Q,S) = \frac{1}{1 + dist(Q,S)}$$

Euclidean Distance

Euclidean Distance is the most common similarity measure in time-series data mining is probably the Euclidean distance [27, 28, 29]. Assuming that two time series, and, are of the same length n, we can think of them as points in n-dimensional space. In this manner we will be able to calculate their distance relying on the differences between the corresponding elements of the sequences as it is shown. Suppose that two time series, $Q = (q_1, q_2, \ldots, q_n)$ and $S = (s_1, s_2, \ldots, s_n)$, both of the same length that equal to *n*, they are points in n-dimensional space. In this manner we will be able to calculate their distance relying on the differences between the corresponding elements of the sequences as it is shown in Equation below:

$$d(Q,S) = \sqrt{\sum_{i=1}^{n} (q_i - s_i)^2}$$

Euclidean distance is that it is very fast to compute, this can be important for low power systems. In the research, I will try to use Euclidean distance as frequently as possible. There are some disadvantages in using this distance as well:

1. Sensitive to scaling and shifting along the *y*-axis. This problem can be solved by normalizing input time series. [30, 31]
2. Both input time series and reference segment must have the same number of points. For this purpose, we will transform the reference time series window to function, this lets us change sampling frequency of reference time series. The other way to solve this is interpolation to equal length.[32]
3. Sensitive to distortions and shifting along the time axis. [33]

Manhattan Distance

For calculation of distance we can apply Manhattan distance between corresponding elements of the time series. In this case we should use this formula.

$$d(T,S) = \sum_{i=1}^{n} |T_i - S_i|$$

Also called "city block distance".

Maximum Distance

Maximum Distance more sensitive to anomalies in time series and calculate maximum distance between two corresponding elements of time series. Maximum Distance can be specified with this formula.

$$d(T,S) = max_{0<i\leqslant n}|T_i - S_i|$$

Minkowski Distance

Also called Lp-norm, Minkowski distance is a more flexible distance. Maximum distance, Euclidean distance and Manhattan distance are particular instances of the Minkowski distance. The formula for this distance can be specified as:

$$d(T,S) = \sqrt[p]{\sum_{i=1}^{n}(T_i - S_i)^p}$$

p - order of Minkowski distance, if :
p = 1: Manhattan distance or *L1-norm*
p = 2: Euclidean or *L2-norm*
$p = \infty$: Supremum or *L3−norm*

Frobenius norm

The Frobenius norm is based on the Euclidean distance. Frequently used in matrix analysis [34]. The Frobenius norm is used to compare the similarity of two matrices.

The Frobenius norm of a matrix X^b *:*

t_r *- the sum of elements on the diagonal of the square matrix*

$$||X^b||_F = \sqrt{\sum_{p=1}^{n}\sum_{q=1}^{T_b}(x_{pq}^b)^2} = \sqrt{tr((X^b)'X^b)}$$

For identical time series Euclidean Distance equal 0.

Dynamic time warping:

Dynamic time warping (DTW) [35] is the most popular technique for similarity measures of time series data. Dynamic time warping reflects the similarity in shape, while

Euclidean distance looks for similarity by timepoints. DTW searches for the best alignment between two time series, attempting to minimize the distance between them.

Given two time series T = $\{t_1, t_2, \ldots, t_n\}$ and S = $\{s_1, s_2, \ldots, s_m\}$ of length n and m, an alignment by DTW method can be contained in a n × m distance matrix:

$$distMatrix = \begin{pmatrix} d(T_1, S_1) & d(T_1, S_1) & \ldots & d(T_1, S_1) \\ d(T_1, S_1) & d(T_1, S_1) & & \\ \ldots & & & \\ d(T_1, S_1) & & & d(T_1, S_1) \end{pmatrix}$$

where distMatrix*(i, j)* corresponds to the distance of the i-th point of *T* and *j*-th point of *S* *d(Ti, Sj),* with $1 \leq i \leq n$ and $1 \leq j \leq m$.

The DTW objective is to find the warping path W = $\{w_1, w_2, \ldots, w_k\}$ of contiguous elements on distMatrix (with *max(n, m)* < *K* < *m* + *n -1*, and w_k = distMatrix(*i, j*)),which minimizes the following function:

$$DTW(T, S) = min(\sqrt{\sum_{k=1}^{k} w_k})$$

An example of DTW alignment is shown in *Figure 4*.

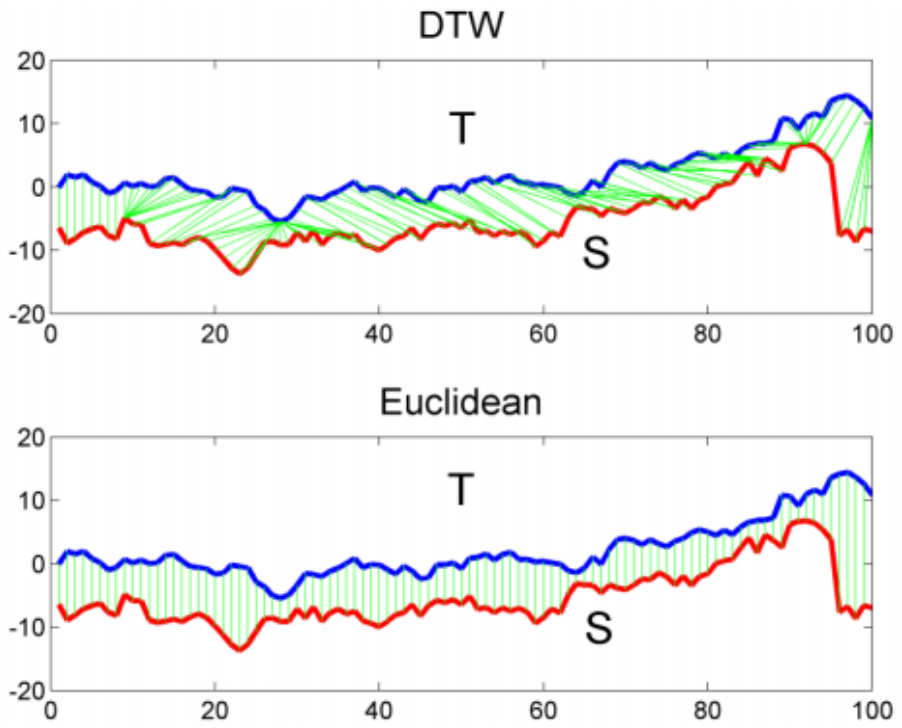

Figure 4*. Comparison of Euclidean distance and DTW (green lines represent mapping between points of time series T and S). As we can see DWT catches the time shift between time series T and S.*

DTW calculation optimization

The warping path can be efficiently computed using dynamic programming [38]. By this method, a cumulative distance matrix γ of the same dimension as the distMatrix, is created to store in the cell *(i, j)* the following value (1):

$$d(T_i, S_j) + min\{\gamma(i-1, j-1), \gamma(i, j-1), \gamma(i, j-1)\} \quad (1)$$

The overall complexity of the method is relative to the computation of all distances in distMatrix, that is *O(nm)*.

The last element of the warping path, w_k corresponds to the distance calculated with the DTW method. In many cases, this method can bring undesired effects. An example is when a large number of points of a time series *T* is mapped to a single point of another time series *S (Fig. 6a, 7a)*. A common way to overcome this problem is to restrict the warping path in such a way it has to follow a direction along the diagonal (*see Fig. 6a, 6b*). To do this, we can restrict Similarity Measures and Dimensionality Reduction Techniques for Time Series Data Mining 79 the path enforcing the recursion to stop at a certain depth, represented by a threshold *δ*. Then, the cumulative distance matrix *γ* will be calculated as follows:

$$\gamma(i,j) = \begin{Bmatrix} d(T_i, S_j) + min\{\gamma(i-1, j-1), \gamma(i, j-1), \gamma(i, j-1)\} & |i-j| < \delta \\ \infty & otherwise \end{Bmatrix}$$

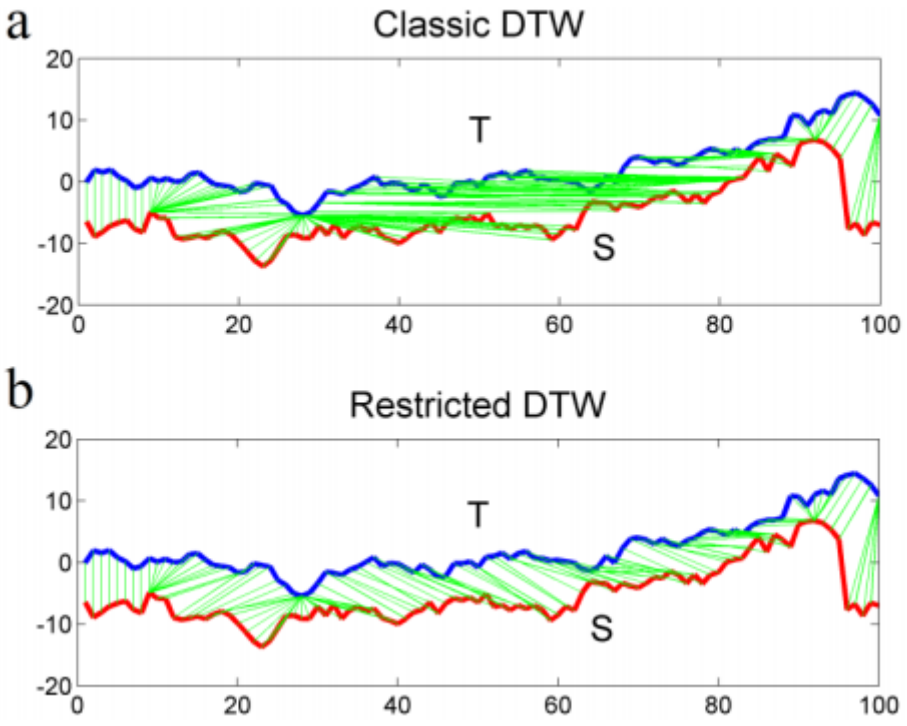

Figure 6. *Difference DTW without threshold δ (a), and with the restrictions in warping path with threshold δ = 10 (b). Green lines match corresponding elements of time series T and S considering time shift.*

This restriction, in addition to limiting extreme or degenerate mappings, allows us to speed up the calculation of the distance DTW, because we only need to adhere to the distance

at a distance of not more than δ positions (horizontally and vertically) from the distMatrix diagonal. This reduces the complexity of computations to *O((n+m)δ)*. The above constraint is also known as the Sakoe-Chiba band (see *Fig. 8a*) [39], and it is classified as a global constraint. Another general global constraint is the Itakura parallelogram (see *Fig. 8b*) [40]. Local constraints are the subject of research and differ from global constraints [41] because they provide local constraints on a set of alternative deep stages of the relapse function:

$$d(T_i, S_j) + min\left\{\gamma(i-1, j-1), \gamma(i-1, j-2), \gamma(i-2, j-1)\right\}$$

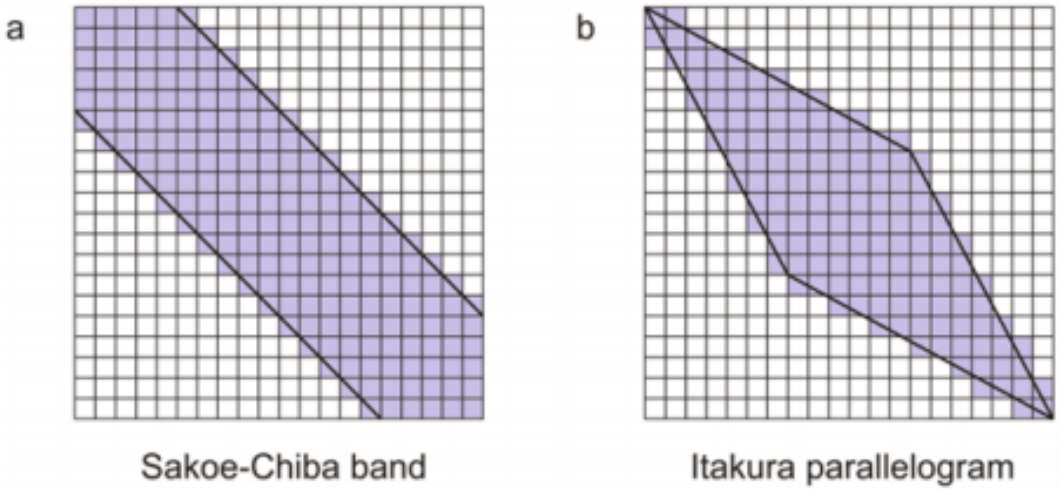

***Figure 8**. Global constraints: (a) Sakoe-Chiba band; (b) Itakura parallelogram.*

Longest Common SubSequence:

Another well-known method that uses the benefits of dynamic programming to allow the comparison of one-to-many points is the Longest Common SubSequence (LCSS) similarity measure. A useful feature of this method is that it is more resistant to noise than DTW, because it allows to not compare some elements of the time series (Fig. 9). This solution creates an LCSS matrix similar to γ, but taking into account similarities instead of distances. Time series T and S of length n and have the recurrence function is expressed as follows with acceptable error *e*.

$$LCSS(i,j) = \begin{cases} 0 & i = 0 \\ 0 & j = 0 \\ 1 + LCSS[i-1, j-1] & if|T_i - S_j| < e \\ max(LCSS[i-1, j], LCSS[i, j-1]) & otherwise \end{cases}$$

The LCSS cell *(n, m)* contains a similarity between *T* and *S*, because it corresponds to the length l of the longest total subsequence of elements between the time series *T* and *S*. To determine the measure of distance, we can calculate with the formula below [42]:

$$LCSS_{dist}(T, S) = \frac{n + m + 2l}{m + n}$$

An example of LCSS alignment is shown in Figure 9

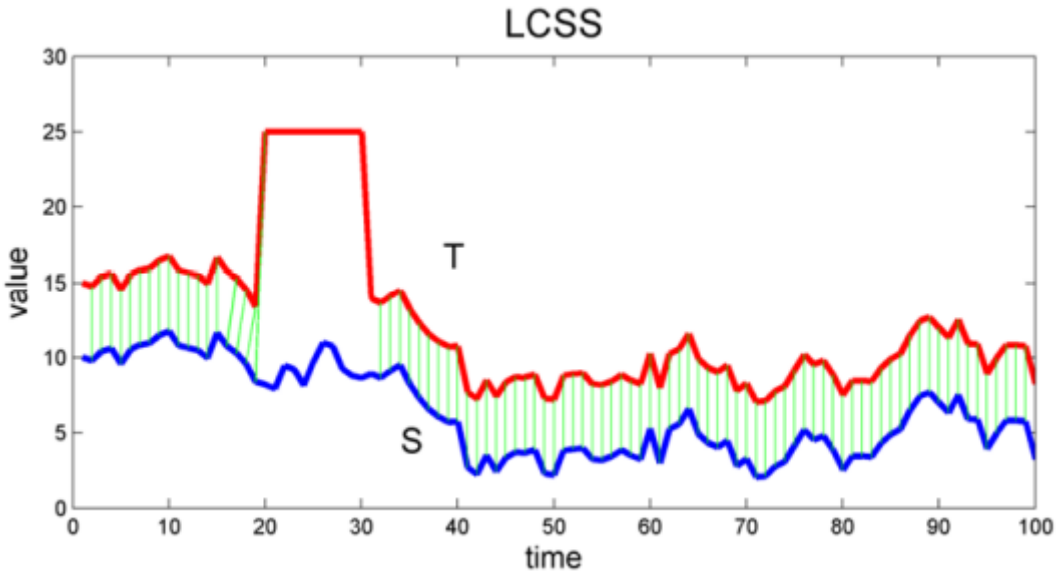

Figure 9 *example of LCSS alignment*

LCSS the time complexity is O(nm), but it can be improved to O((n + m)δ) if a restriction is used (i.e. when |i - j| < δ).

Principal Component Analysis (PCA) similarity factor

PCA is one of the most popular techniques for dimensionality reduction techniques. It is a linear transformation that projects the original data into a new coordinate system with minimal information loss. In multidimensional cases, information is the structure of the source data, i.e. the correlation between the features and the change in the structure of the correlation between them. To create a projection, the PCA selects the coordinate axes of the new coordinate system one after the other according to the largest variance of any projection. The PCA similarity coefficient is determined with this formula:

$$S_{PCA}(X^b, X^c) = tr(L'MM'L)$$

where L and M are matrices containing the first l principal components X^b and X^c. This means that the principal components are calculated according to a standard algorithm using the matrices $(X^b)\ '\ X^b$ *and* $(X^c)\ '\ X^c$, and then l principal components with the highest eigenvalues are selected.

For identical time series Matrix PCA similarity factor equal 1.

Convolutional neural network:

CNN (Convolutional Neural Network) takes a tensor as its input. The input then sequentially goes through the layers of the model. One processing step is usually called a layer, which could be a convolution layer, a pooling layer, a normalization layer, a fully connected layer, a loss layer, etc.

Abstractly CNN structure can be described as a scheme in *Figure 10*

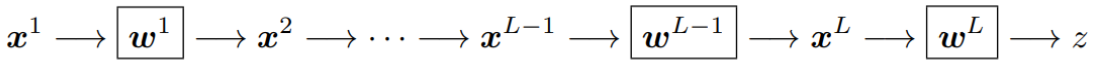

Figure 10. *Example of CNN structure*

In Figure 10, x^1 is input that has been prematurely transformed into a tensor. It goes through the first layer, which is the first box. After the first layer we receive output x^2, which also acts as the input to the second layer x^1 processing.

This processing continues until the end of all layers in CNN, which produces x_L. However, another layer is added for the reverse propagation of errors, a method that studies the good values of parameters in CNN.

The last layer is a loss layer. Let us suppose t is the corresponding target (ground-truth) value for the input x^1 , then a cost or loss function can be used to measure the discrepancy between the CNN prediction x^L and the target t. For example, a simple loss function could be :

$$z = \frac{1}{2}||t - x^L||^2$$

Weights and Basis

Weights and bases are both learnable parameters in the network. Neural network randomizes the values of weight and displacement before training. As the network learns, both parameters are adjusted to optimal values and the correct result. The two parameters differ in the degree of their impact on the input data. Bias represents how far predictions are from their intended value. In our case filters of CNN contain weights.

The ReLU layer

A ReLU layer does not change the size of the input, that is, x_1 and y share the same size. In fact, the Rectified Linear Unit (hence the name ReLU) can be regarded as a truncation performed individually for every element in the input:

$$y, j, d \;=\; max\{0,\; xl\, i, j, d\}\,,$$

with 0 ≤ i < H_l = H_l+1, 0 ≤ j < W_l = W_l+1, and 0 ≤ d < D_l = D_l +1.There is no parameter inside a ReLU layer, hence no need for parameter learning in this layer.

$$\frac{dy_{i,j,d}}{dx^l_{i,j,d}} = [x^l_i, j, d > 0]$$

Where J·K is the indicator function, being 1 if its argument is true, and 0 otherwise.

Hence, we have

$$\left[\frac{dz}{dx^l}\right]_{i,j,d} = \left\{ \begin{array}{cc} \left[\frac{dz}{dy^l}\right]_{i,j,d} & if\ x^l_{i,j,d} > 0 \\ 0 & otherwise \end{array} \right\}$$

In other words, the function max(0, x) is not differentiable at x = 0. The purpose of ReLU is to increase the nonlinearity of CNN. The ReLU function is illustrated in Figure 11.

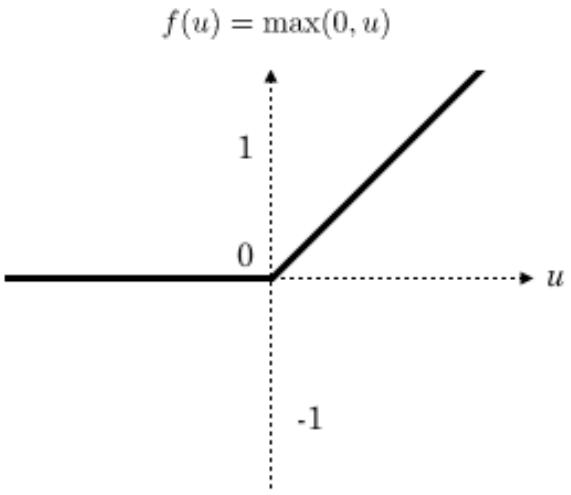

Figure 11 ReLu activation function graph

Back-Propagation Algorithm

Back-propagation is used to train neural networks. Back-propagation algorithm allowed to calculate the gradient for each weight in the network model. Optimization algorithm use gradient to update the model weights.

- Error Function: Loss function that is minimized while training the process of a neural network.
- Weights: Parameters of the network taken as input values to the loss function.
- Error Gradients: First- parameters.

The algorithm involves the recursive application of the chain rule[109] that is used to calculate the derivative.

Autoencoder

In simple word autoencoder it is two Neural Networks connected together. The output of one first Neural Network serves as an input for a second Neural Network. Fits Neural Network so called encoder and second neural network decoder. There are a lot of autoencoder architectures. The most straightforward version of autoencoder does the task of regenerating the input at the output. The application of such kind of model is to extract latent features at the hidden layer and then reconstruct the same input. The hidden layer is used to extract the features from the input data in order to catch patterns in original data. [43][44]. Feature of the network is that the number of hidden units is much less than the actual I / O units. The reason for training is to make the model correctly compress used data and then reconstruct it by a neural network, training process includes adjustion of the weights in a neural network. Mainly it is done in face recognition applications where the different facial expressions pose a problem for verifying the image.

One of the most common tasks for the autoencoders is denoising. Denoising autoencoders are used to extract denoised data output from a noise input. The input provided is used to predict at the output layer in presence of noise at the hidden layer. DAE learn more efficiently and are more susceptible to noise. Denoising autoencoders are used to train using simple back propagation algorithms in different variations of it. [43][44]

Biosensors

Tme miniaturization of sensors, have significantly contributed to commercializing wearable technology. Most of the standard commercially available sensors are either mechanical or optical, but nowadays transdermal microneedles also are getting used for micro-sensing like continuous glucose monitoring. However, there remain certain challenges that require to be addressed before the likelihood of large-scale deployment. the largest challenge faced by of these wearable sensors is our skin, which has an inherent property to resist and protect the body from the surface world.

Recent advances in fabrication and packaging techniques enables to embed an unlimited number of microelectronic devices and sensors on a cut a awfully low cost.

This has significantly reduced the healthcare costs and has improved continuous monitoring of important parameters, especially for athletes, thus improving their performance [45]. the longer term of remote biomedical sensing are further transformed with the rolling out of 5G networks, combined with technologies like the web of things (IoT), machine learning, and AI [46].

Wearable technology can help individuals track their vital physiological parameters; with the choice to consult a doctor only needed [45,47]. a decent indicator of the advantages of wearable technology is that the day-by-day increasing demand for private diagnosis and monitoring [48]. Its usage is currently not limited to watch glucose levels, but has recently been proposed as an alternate method to perform fast HIV diagnoses [49], early detection of Alzheimer disease [50], and perspiration monitoring through wearable paper-based sweat sensor [51], thus leading personalized medicine to a brand new level [52]. Miniaturization of microelectronics together with stretchable microelectronics and telecommunication enables the assembly of wearable sensors resulting in many novel clinical applications. Wearable technology consists of three processes: sensing, processing, and wireless transmission of information [53]. processing may be a crucial step because it involves noise reduction and have extraction of clinically relevant physiological data [54]. One such example is that the flexible electrocardiograph (ECG) sensor shown in Figure 15 B. Currently, sensing technology isn't only limited to electrophysiological measurements like ECG, electromyography (EMG), or electroencephalography (EEG), rather, it's expanded to electrochemical, electromechanical, and transdermal (minimal invasive by measuring fluid in between tissue) sensing [55].

Skin: First Defence of the Immune System

Skin can be divided into several separate layers: the hypodermis (deepest layer), the dermis, and also the epidermis (superficial layer) as shown in Figure 12.

Key factors that causes interference for sensing through the skin:

- Resistance to Mechanical Sensing [56-58].
- Attachment of Sensors to the Skin [59-63].
- Stretching of the Skin [64- 67].

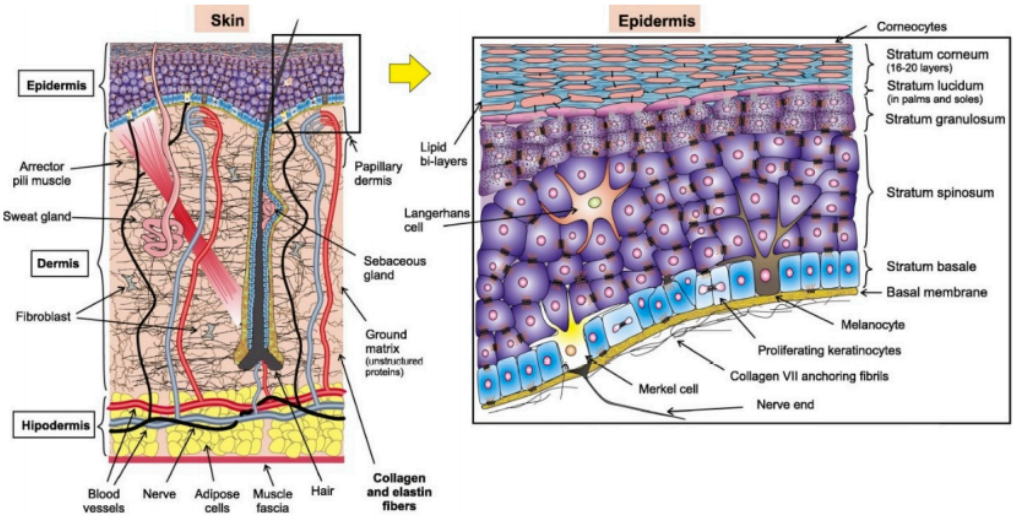

Figure 12.Illustration of the different layers of the skin.

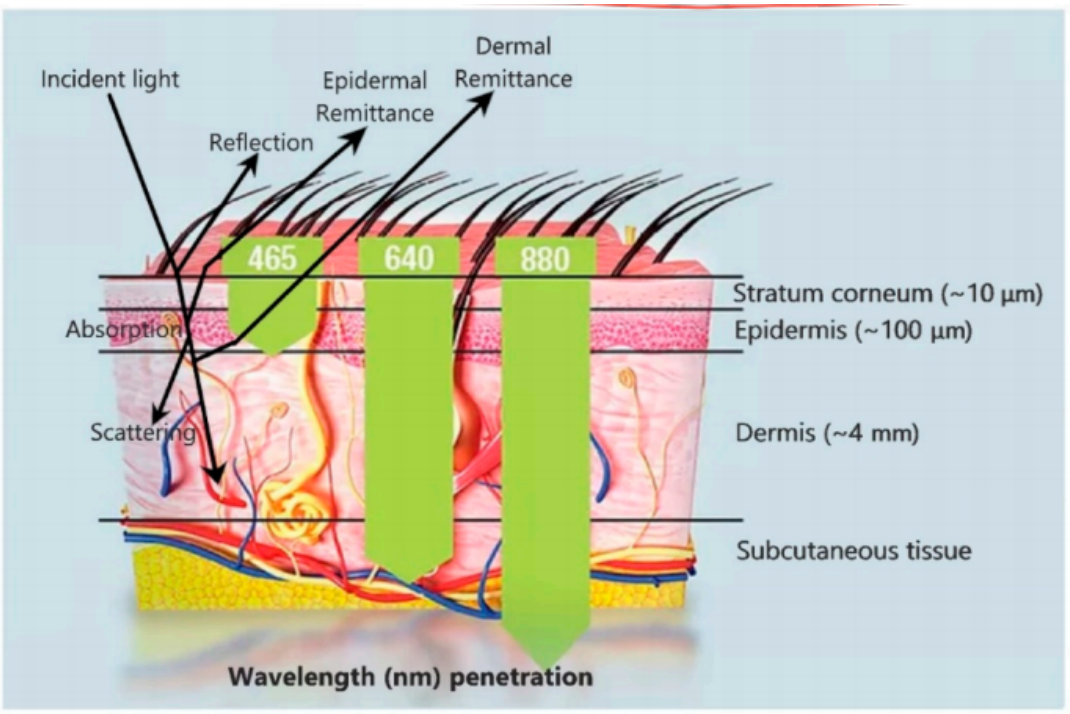

Figure 13. *Incident light shows reflection, absorption, and scattering phenomena at different locations in skin layers, (Green downward pointing arrows). Light penetration into the skin with respect to its wavelength.*

Wearable Sensors:

There are several types of wearable sensors currently in use. Three major and commonly used types

- Transdermal microneedles,
- Optical sensors
- Mechanical sensors

Transdermal Microneedles

The prevalent utilization of microneedles to this point has been for transdermal drug and vaccine delivery [68]. Application of microneedles as diagnostic sensors by accessing the interstitial fluid [69–71]. Transdermal sensing has high importance because they have the ability to obtain real-time clinical data for health monitoring. The Figure of the microneedles system for fluid extraction is shown in *Figure 14*.

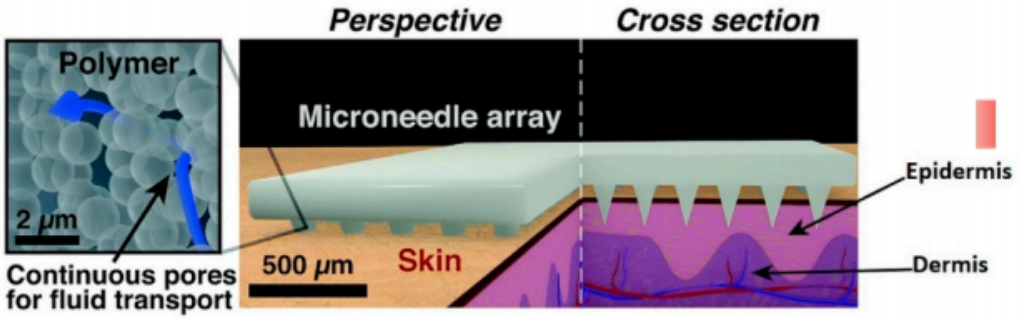

Figure 14*. Schematic diagram of microneedles inserted into the skin for interstitial fluid extraction.*

Measurements that can be obtained ISF (interstitial fluid). The ISF can be used for immune system monitoring [73-81].

The most common optical sensors used in wearable electronics are used to detect oxygenation of blood and heart rate monitoring [84,85]. In diagnosing any clinical or biological event, the absorption and scattering

- *Optical Sensors*

The most common optical sensors used in wearable electronics are used to detect oxygenation of blood and heart rate monitoring [84,85]. Optical sensors are being utilized in a wide variety of applications [86,87–93].

Photoplethysmography (PPG)

Photoplethysmography (PPG) is the optical technique that can be utilized to quantify blood volume. It has a popular clinical application and innovation, used in financially accessible medicinal gadgets, in particularly , for pulse oximeters and digital blood pressure monitors for heart beat detection. The fundamental type of PPG only requires a couple of optoelectronic parts: a light source (typically mounted on the skin as shown in Figure 15(A), to transmit light into the skin, and a photodetector to detect the light intensity variation related to the changes in volume (Figure 15B). PPG is a non-invasive technique it uses at a

infrared or red wavelength (see Figure 13). The most perceived extracted features are the peripheral pulse waveform and are synchronized to every heartbeat (Figure 15C).

The light interaction with biological tissue has already been investigated comprehensively by Anderson and Parrish in 1981 [94]. Some scientists have examined the optical procedures related to PPG estimations [95–102].The example of a PPG signal extracted from a different location in the body is given in *Figure 15 (D)*

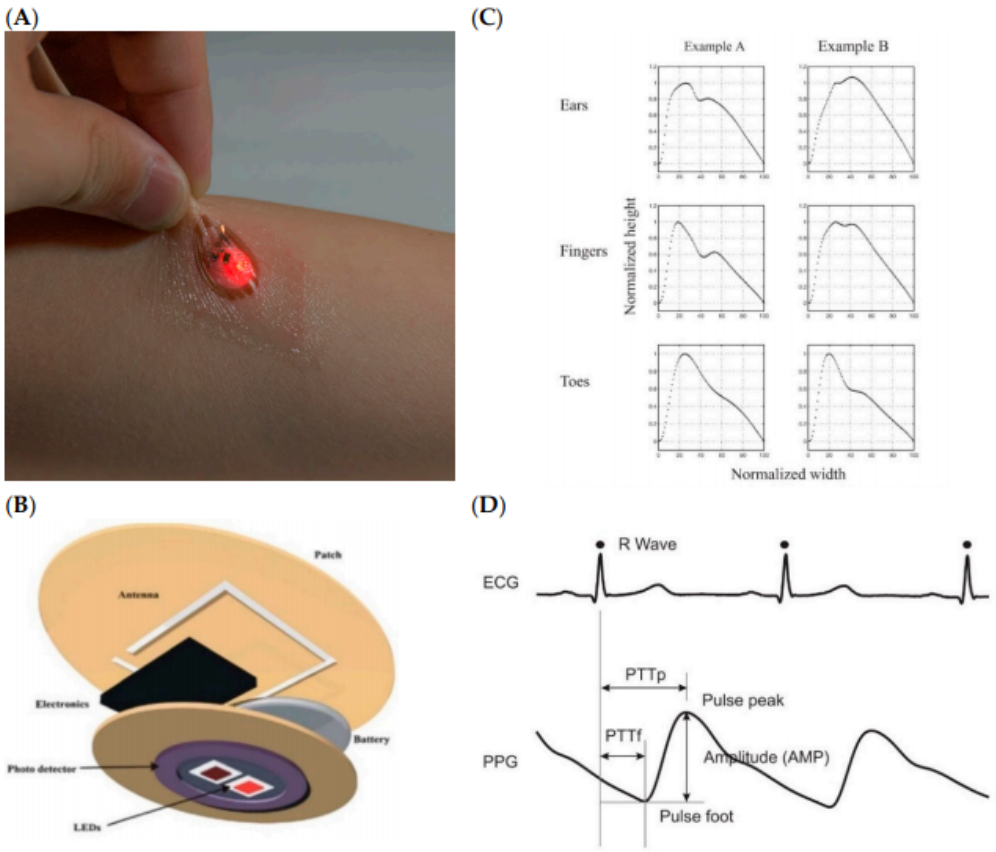

***Figure 15**. (A) Optical sensor mounted on skin, (B) Basic diagram of a wireless photoplethysmography (PPG) sensor, (C) PPG signal collected from three different locations, (D) Comparison of the PPG signal with ECG signal*

Currently, many researchers are exploring this technique due to its cost-effectiveness, accessibility, portability, simplicity or ease of use in clinical settings. PPG-based innovation can be found in an extensive variety of economically accessible medicinal gadgets for measuring pulse, oxygen saturation, cardiovascular output,blood pressure and peripheral diseases.

Electrocardiogram (ECG)

An electrocardiogram (ECG) is a measure of how the electrical activity of the heart changes over time as action potentials propagate through the heart during each cardiac cycle. However, it is not a direct measure of cellular depolarization and repolarization in the heart, but rather the relative, cumulative size of the populations of cells that produce changes in their membrane potentials at a given time; it shows the electrical differences throughout the heart when depolarization and repolarization of these atrial and ventricular cells occur.

Electrical axis and recording lead vectors .

The ECG is measured by placing electrodes on the patient's skin - it is also called a "surface ECG".The wave of electrical depolarization propagates from the atria down through the IVS to the ventricles. Therefore, the direction of this depolarization is usually from the upper to the lower side of the heart. The direction of the direction of the depolarization wave is usually to the left because of the leftward orientation of the heart in the thorax and the greater muscle mass of the left ventricle than the right. This general direction of motion of electrical depolarization through the heart is referred to as the electrical axis

The basic principle of ECG recording is that when the depolarization wave moves to the recording it leads to a positive or upward deviation. When it deviates from the record assignment, it results in deviation or downward deviation.

The electric axis is usually directed down and to the left, but we can evaluate it more accurately in individual patients if we understand from what is the "direction" of each lead recording is measured by the ECG.By agreement, we record a standard surface ECG using 12 different ones a record of the leading "directions", although only 10 records are quite confusing this requires electrodes on the skin. Six of them are registered from a thorax lying over the heart - a thorax or precordial assignment.

Four recorded from the limbs - limb withdrawal. It is important that every 10 recording electrodes are placed in the correct position, otherwise the appearance of the ECG will change significantly, preventing correct interpretation.

Normal ECG

From the above, it can be seen that the first structure to depolarize during normal sinus rhythm is the right atrium, closely followed by the left atrium. Therefore, the first electrical signal on a normal ECG originates from the Atria and is referred to as a P wave. Although there is normally only one P wave in most leads on an ECG, the P wave is actually the sum of the electrical signals from the two atria, which normally overlap.

There is then a brief, physiological delay as the atrioventricular (AB) node slows down the electrical depolarization slows down before it is transmitted to the ventricles. This delay is responsible for the PR interval, a short period in which no a short period in which no electrical activity is seen on the ECG, represented by a straight horizontal or "isoelectric" line.

Depolarization of the ventricles usually yields the largest portion of the ECG signal (because of the greater muscle mass in the ventricles) and this is called the QRS complex.

- The Q wave is the first initial downward or "negative" deflection.
- The R wave is then the next upward deflection (assuming it crosses the isoelectric line and becomes "positive").
- The S-wave is then the next deflection downward, provided it crosses the isoelectric line and briefly becomes negative before returning to the isoelectric baseline.

In the case of the ventricles, there is also an electrical signal that reflects the repolarization of the heart muscle. This is represented by the ST segment and the T wave. The S-T segment is usually isoelectric, and the T wave in most leads is an upright deflection with variable amplitude and duration (see *Figure 16*).

Normal intervals

The recording of an ECG on standard paper enables the time taken for the different phases of the electrical Depolarization phases to be measured, usually in milliseconds. There is a recognized normal range for such "intervals":

- PR interval (measured from the onset of the P wave to the first deflection of the QRS complex). Normal range 120 - 200 ms (3 - 5 small squares on the ECG paper).
- QRS complex to the end of the QRS complex at the isoelectric line).Normal range up to 120 ms (3 small squares on ECG paper).
- QT interval normal range up to 440 ms (may be slightly longer in women and varies with heart rate)

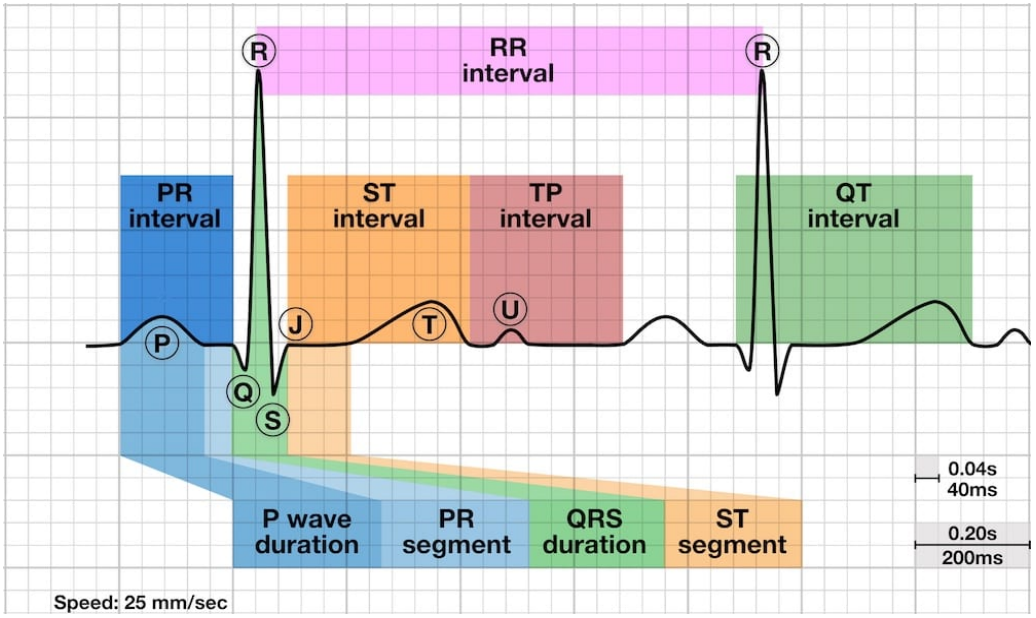

***Figure 16**. ECG cardiac cycle*

Modern sensors capabilities

In order to choose a combination of physiological time series which is possible to obtain simultaneously using wearable device I searched for developing sensors from fronto sensor providers. List flagship healthcare sensors producers I found in paper Wearable Technology 2016-2026[8]. As an example of a device that can produce multidimensional physiological time series I choose TIDA-01580 from Texas Instruments. This device is a simple, portable, multi-parameter patient monitor device, for synchronized ECG and PPG measurements. Raw data is available to the user for calculation of heart rate, blood oxygen concentration (SpO2), pulse transit time (PTT) and ECG.

Conclusions

There is an increasing interest in studying various aspects of time-series. Especially in recent years, due to integration of big data technologies, higher usage of sensors, and ability to analyse video data and other signals they are becoming more and more accessible for analysis. The increasing volume of data requires specific tools to be analysed, along with classical data mining techniques similarity measure techniques can be used in detection of

anomalies, searching for specific wave forms of time-series. Combination of anomaly detection can significantly save computational resources and increase the effectiveness in both.

There is a clear grooving necessity and availability of wearable biosensors on the healthcare market. They can help provide better and cheaper treatment to patients, help seniors or people who live in remote places, and reduce insurance prices. Besides being a solution, wearable sensors are also a part of today's trends in medicine. Usage of wearable sensors within Telehealth programmes can be included in insurance packages. This can guarantee price reduction for monitoring people with light diseases, reduce pressure on physicians, and can reduce health insurance prices.

Experimental results

Data

Combined measurement of ECG, Breathing and Seismocardiography

To build the database, 20 presumed healthy volunteers were measured. During the measurement, subjects were asked to be in a relaxed position on a comfortable regular single bed and not to sleep. After connecting the sensors, we recorded the basal state of the subjects, measuring for 5 minutes. After that, the subjects began to listen to classical music for about 50 minutes. Finally, we watched all the subjects for another 5 minutes after the end of the music.

Data has been obtained using a Biopac MP36 data acquisition system.

- Channels 1 and 2 of the system were designed to measure a normal ECG (leads I and II, respectively) with a bandwidth of 0.05 Hz to 150 Hz.
- Channel 3 was used to measure the respiratory signal received from the thoracic piezoresistive band (sensor SS5LB from Biopac , Santa Barbara, California, USA) with a bandwidth of 0.05 Hz to 10 Hz.
- Channel 4 was designed to receive SCG using a three-axis accelerometer (LIS344ALH, ST Microelectronics) and a bandwidth of 0.5 Hz to 100 Hz . To measure the ECG, we used control electrodes with foam tape and adhesive gel (3M Red Dot 2560). Each channel was selected at a frequency of 5 kHz.

MIMIC-III Clinical Database

MIMIC-III is a large, freely available database that includes de-identified health-related data related to more than 40,000 patients who were in the first aid units of Beth Israel Medical Center in 2001. The database contains information such as demographics, bed measurements (~ 1 point per hour), laboratory results, procedures, medications, caregiver notes, imaging and mortality reports (including hospital discharge).

MIMIC supports a variety of analytical studies covering epidemiology, improving clinical solutions, and developing electronic tools. It is notable for three factors: it is freely available to researchers around the world; it covers a diverse and very large population of resuscitation patients; and it contains very detailed data, including vital signs, laboratory results, and medications.

MIMIC-III combines deidentified, comprehensive clinical data from patients admitted to Deaconess Beth Israel Medical Center in Boston, Massachusetts, and makes it widely available to researchers internationally under a data use agreement. The open nature of the data allows clinical trials to be replicated and improved in ways that would otherwise be impossible.

The MIMIC-III database was populated with data obtained during routine hospital care, so there was no associated burden on caregivers and no interference with their workflow. Data were downloaded from several sources, including:

- archives of critical information information systems.

- database of electronic medical books of the hospital.
- The main file of death of the Social Security Administration.

MIMIC-III Waveform Database

The MIMIC-III signal database contains 67,830 record sets for approximately 30,000 resuscitation patients. Almost all record sets include a signal recording containing digitized signals (usually including ECG, blood pressure, respiration, and PPG, and often other signals) and a "numerical" record containing time series of periodic measurements, each of which is a quasi-continuous recording of vital signs of one patient during the entire period of stay in intensive care (usually several days, but duration - several weeks). A subset of this database contains signal records and digital signals that corresponded to and matched the MIMIC-III clinical database records.

The MIMIC-III Waveform Database contains recordings of multiple physiologic signals and time series collected from bedside patient monitors in adult and neonatal intensive care units (ICUs).

The MIMIC-III Waveform database is a subset to the MIMIC-III clinical database[103], which contains detailed clinical information on most patients presented in the Waveform database [104]. Because the contents of each database were collected independently, in part in an identified form, matching clinical data to signal data is a non-trivial task, and only a subset of the Waveform Database records corresponds to clinical database records.

Recorded signals and time series vary depending on the choice of resuscitation staff. Waveforms almost always include one or more ECG signals, and often include continuous blood pressure (BP) waveforms, photoplethysmogram (PPG) signals, and respiration with additional waveforms (up to 8 simultaneously). Digits typically include heart rate and respiration, SpO2, and systolic, mean, and diastolic blood pressure, and others, if available. Recording time also varies; the duration of most is a few days, but some are shorter and others are a few weeks.

Technical Limitations

Gaps and patient identification:

Signal forms and digital records were removed from raw data dumps collected from bedside monitors using equipment provided by the monitor manufacturer. Raw data dumps contain data files collected from a single patient monitor during a single monitoring session (which can last days or weeks). Typically, the monitoring session ends when the patient is discharged, so that the data in one file comes from one patient. However, sometimes the monitor is not reset when the patient is discharged, and the session continues after receiving a new patient; in this case, the raw data file contains data from two (or more) patients with a gap (interval during which no signals or numbers are recorded), which usually lasts an hour or more. Such gaps can also occur if the monitor is temporarily turned off (for example, for a laboratory test) and then connected to the same patient. Because raw data files usually do not contain patient IDs, it is easy to determine exactly whether data before and after a break were collected from the same patient.

Ideally, each MIMIC-III signal database entry should contain data from only one patient. All raw data files containing intervals of one hour or more were split into separate records to reduce the likelihood that any record contained data from multiple patients. The current project is to study the record sets created in such a way, if possible matching them with the records of the MIMIC-III clinical database, to determine whether and how to collect them.

Wave alignment problems:

The method used to extract MIMIC signal data was not developed for interwave analysis. The signal data contains undefined / unknown filtering delays and /or unknown delays between channels, which may not be constant in this record. Therefore, although the ECGs are synchronized with each other in time, between any other waveform in the data there may be (changes) a delay of up to 500 ms. For example, the pulse travel time measured between different waveforms may be unreliable (either in absolute or relative terms).

ECG limitations:

ECG signals in the signal recordings were first taken with 12-bit accuracy with a high sampling rate, and then scaled and decimated to 500 samples per second (per signal). Scaling reduced the effective amplitude resolution from 12 bits to 9 or 10 bits in typical cases and only 7 bits in some cases. From each set of 4 consecutive decimated samples of the same ECG signal, one was recorded (selected using a turntable compressor, a technique sometimes referred to as "peak selection"). The result is an ECG signal that is taken 125 times per second, but at intervals ranging from 2 to 14 ms (average 8 ms). Since the interval between any given pair of samples was not available to us, the reconstruction of ECG signals provides uniform intervals of 8 ms. These reduced-time, amplitude-resolution signals, as well as the jitter sampling introduced by "peak selection", were the only ECG signals that could be recorded from ICU monitors. Although ECGs reconstructed in this way can be easily interpreted visually, they are not suitable as input data for certain algorithms for ECG analysis, especially those that are sensitive to the characteristics of the signal in the frequency domain. Note that these restrictions apply only to ECG signals and not to other signals that were initially taken at regular intervals of 8 ms (125 samples per second) and were not scaled to capture.

MIMIC-III Waveform Database Matched Subset

The corresponding subset of the MIMIC-III Waveform Database contains 22,317 signal records and 22,247 digital records for 10,282 individual patients in the intensive care unit. These recordings typically include digitized signals such as ECG, blood pressure, respiration, and PPG, as well as periodic measurements such as heart rate, oxygen saturation, systolic, mean, and diastolic blood pressure.

This database is a subset of the MIMIC-III signal database representing those records for which the patient is identified, and their corresponding clinical records are available in the MIMIC-III clinical database.

Only a subset of signal records actually contained enough information to reliably identify the patient, and not all of them coincided with the time period presented by the

MIMIC-III clinical database. Using all available information, a total of 22,317 signal records (34%) and 22,247 digital records (35%) were identified that could be linked to the patient in the clinical database, through a process of predominantly automated coordination with some manual corrections.

Data sample from random patient is shown in *Figure 17.*

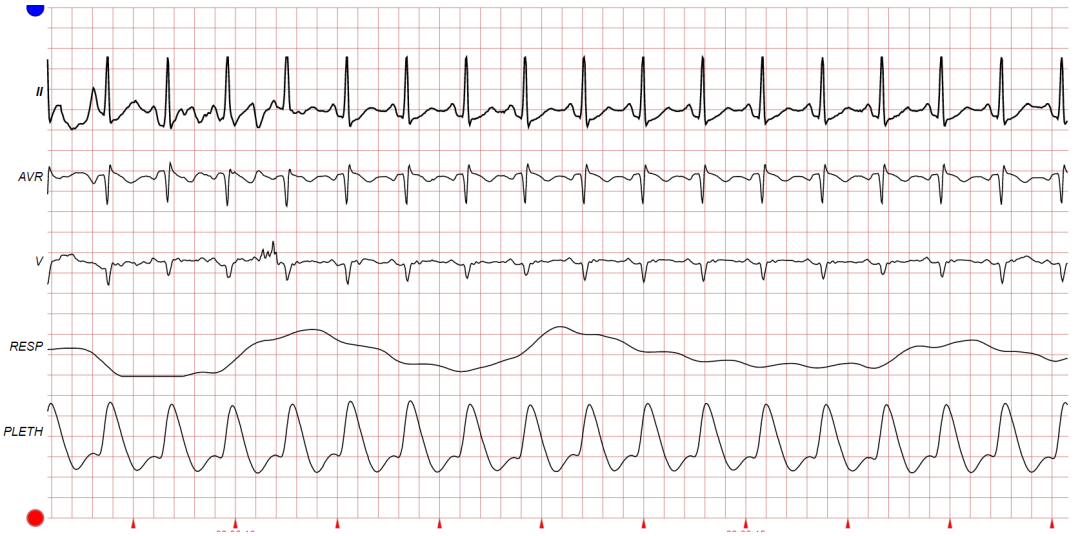

Figure 17*.Sample from MIMIC-III Waveform Database Matched Subset*

Data preparation

The main dataset I worked with is the MIMIC-III Waveform matched subsets dataset, this dataset used to perform analysis and detect abnormalities in ECG data using PPG data as augmented data. PPG should improve accuracy and reduce 'false-alarms', increase speed which is critical for streaming applications.

ECGs have different sampling, it depends on the device using which they were obtained. In our case 'MIMIC-III Waveform matched subsets' dataset frequency is 125 Hz while for 'Combined Measurement of ECG, Breathing and Seismocardiography' dataset sampling rate is 5000hz. Signals down-sampled to 100Hz produced acceptable results for time-domain analysis and Poincaré plots, but not for frequency-domain analysis. To make the framework work faster I downscaled signals from 5000hz to 125hz for 'Combined Measurement of ECG, Breathing and Seismocardiography' dataset. This lower frequency allowed me to make calculations more simple and save accuracy at the same time.

Data for processing

MIMIC-III Waveform matched subsets dataset are represented as a continuous time series. To make analysis more simple I extracted R-R intervals from time series. To obtain these segments I used a sliding window approach. Window try to catch three or four cardiac cycles and detect R-peaks using 'neurokit2'[105] Python library, then cut in to R-R intervals (see *Figure 18*).The window has length of four seconds and padding with the length of 300ms, padding is used for better R-reaks detection in order to avoid false peaks detection. Then these boundaries also apply for PPG time series.(see *Figure 19*).

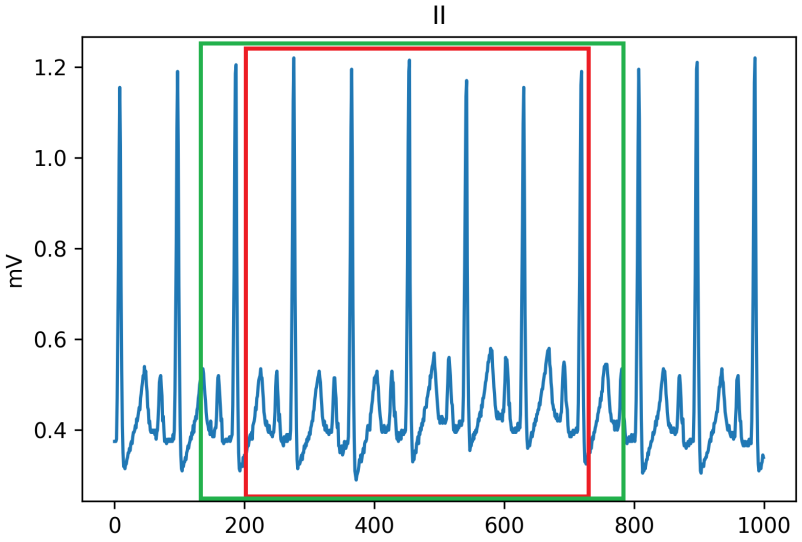

Figure 18. *Sample form streaming time series, red lines show window boundaries for R-R segments detection, green lines show boundaries of data to read for window.*

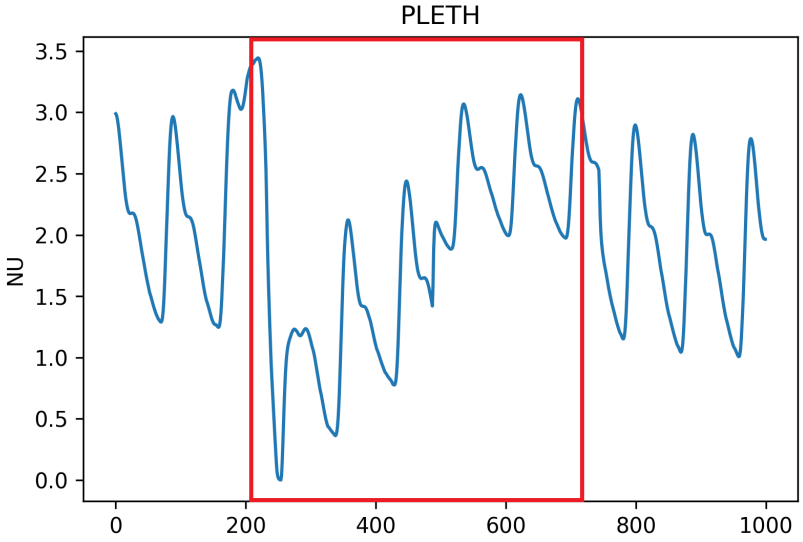

Figure 19. *PPG sample for processing that corresponds to window in Figure 18*

I took about 8 hours of ECG recording with a few anomaly pieces which are caused by incorrect usage of the sensor. This evaluation dataset contains ECG and PPG segments (see *Figures 20 and 21).* As we can see PPG data have much more anomalies, PPG waveform will be used as supplementary sources of information for ECG anomalies detection. This can significantly Improve reliability and reduce 'false alarms'.

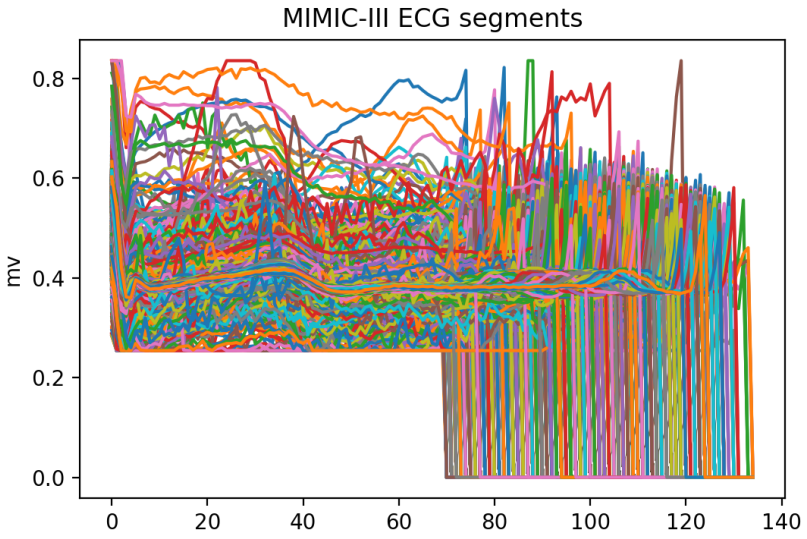

Figure 20. *Sample of ECG segments data for evaluation*

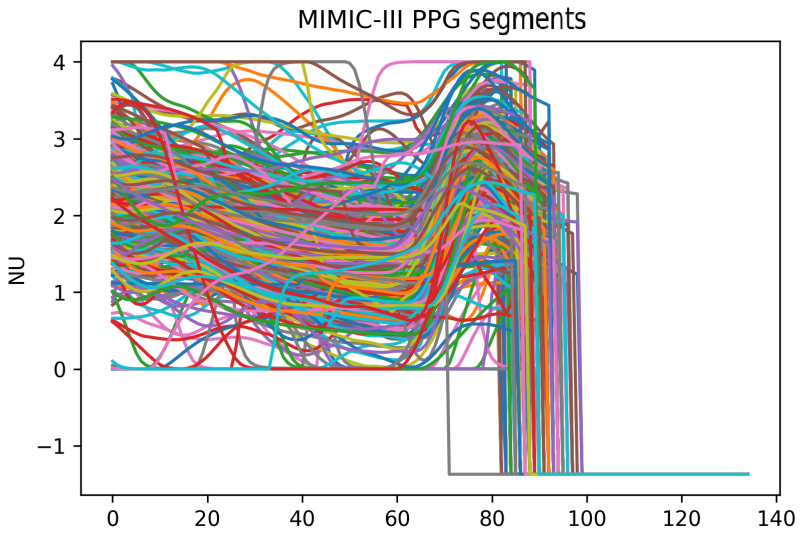

Figure21. *Sample of PPG segments data for evaluation*

Data for training Autoencoder

Combined measurement of ECG, Breathing and Seismocardiography dataset is a clean dataset with ECGs obtained from healthy patients in perfect conditions. All patients in this dataset are presumably healthy and have normal ECGs. I used this data for model training. After splitting data into R-R intervals I received segments which you can see in *Figure 22(A)* . Both Similarity measure and convolution Autoencoder anomaly detection are based on data in this format.

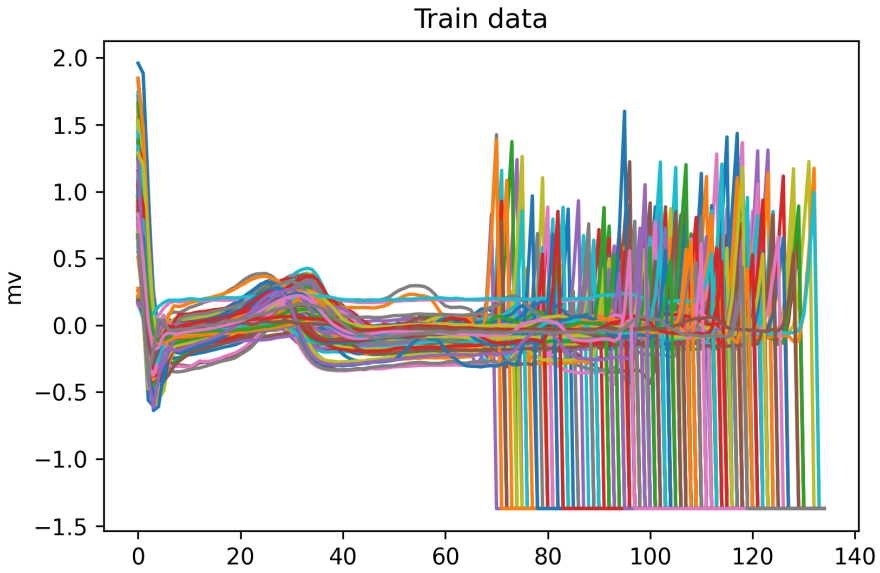

***Figure 22**.A . Segment of train data*

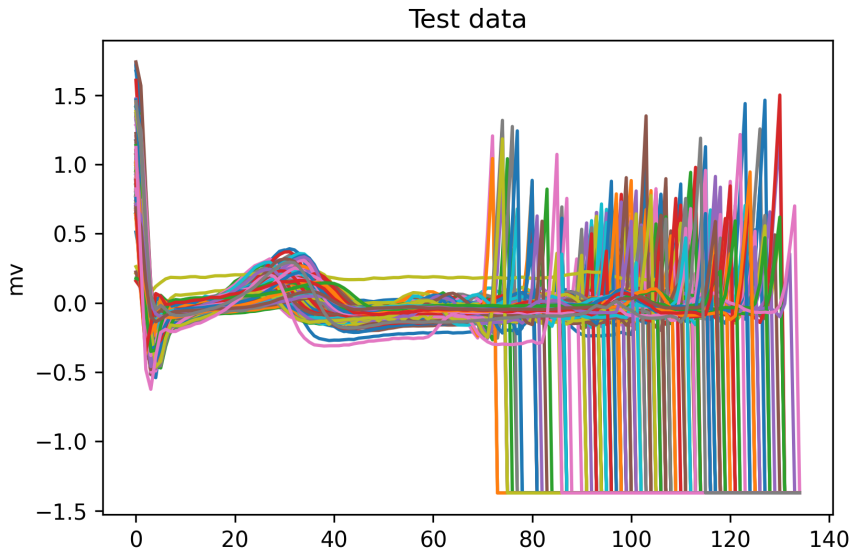

***Figure 22**.B . Segment of test data*

Autoencoder train data is used for both training and testing, the test dataset is used as validation for validation loss estimation.

Scaling

I used a Min-Max scaler. This scaler allowed me to increase accuracy significantly. All zero values after the end of the second R peak were changed to Min volt value. Interval for Min-Max scaler is from zero to one. Also scaling allows us to use the Relu activation function, because this activation function doesn't work on values under zero.

Exploratory data analysis

There are some common problems for ECG anomaly detection, one of them is significant variation of cardiac cycle structure, different people have different ECG curves. ECG this can depend on age, body mass, gender or even climate. There are some particular cases in the 'Combined Measurement of ECG, Breathing and Seismocardiography' dataset (see Figure 23). As we can see the difference between cardiac cycles of two people can be very significant, this makes anomaly detection even more challenging, because the same ECG segment can be normal for one person and at the same time can be considered as anomaly for another.

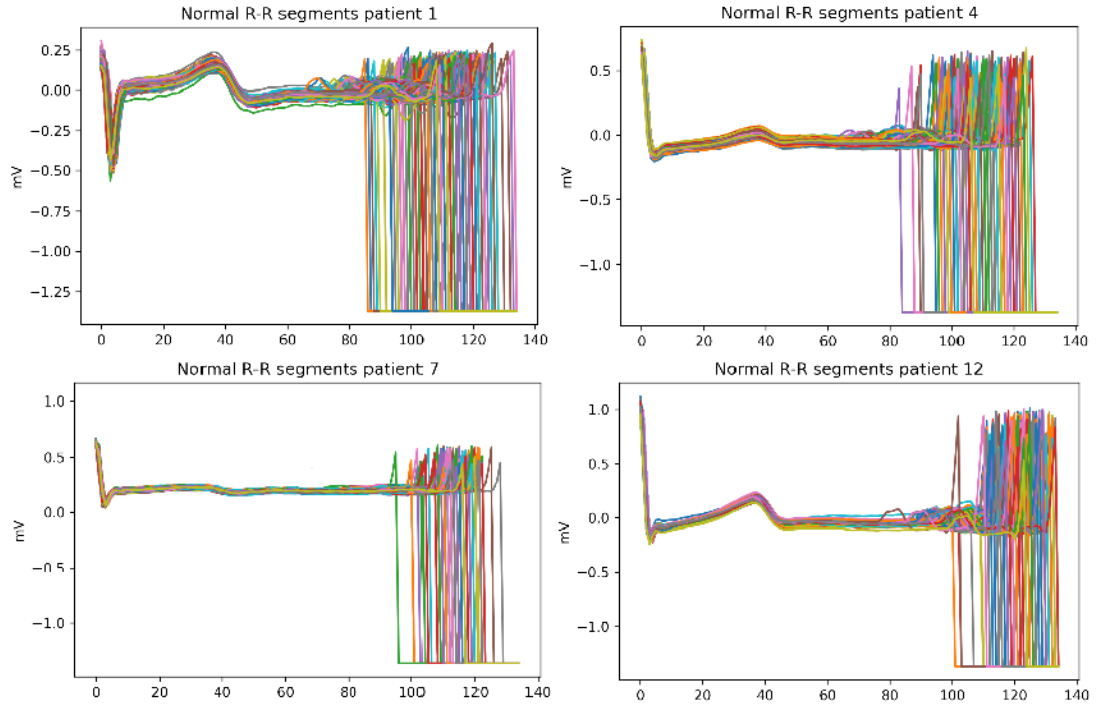

Figure 23. *Variation in the structure of cardiac cycles between different people* .

Differences can be so significant that similarity measure approaches can reliably work only if unique specifics of the observed person are taken into consideration. That's why I obtain a common ECG segment for each person individually and refresh it if 'false-alarm' occurs.

The devices which were used for ECG screening are also critical. Some of them have different sensitivity and noise levels. I had to consider this factor for choosing similarity measure techniques and the configuration of layers in Deep Autoencoder.

Combined measurement of ECG, Breathing and Seismocardiography

As I have mentioned before, the difference between healthy ECG segments of different people can be significant, this nicely Illustrated in *Figure 23*. But for the same person variation mostly minore and affects the length of the cardiac cycle.

MIMIC-III Waveform matched subsets

Compare to Combined Measurement of ECG, Breathing and Seismocardiography' dataset MIMIC-III Waveform matched subsets is much more noisy and include a lot of of

easily visible anomalies along with segments which are close to normal but they have some P-waves,T-waves or R-peaks which are lower than normal. Second type of anomaly is more interesting for us because it is harder to detect and estimate the index of abnormality. I used unsupervised learning techniques in order to make this reamevork more flexible and describe about a level of abnor based on this index, later we can set a threshold for this index and ignore abnormalities these are insignificant, alo very high index can be considered as abnormality caused by incorrect usage(bad contact of skin with sensor etc.) or more severe hearth instability. Final data for evaluation is shown in *Figure 24.*

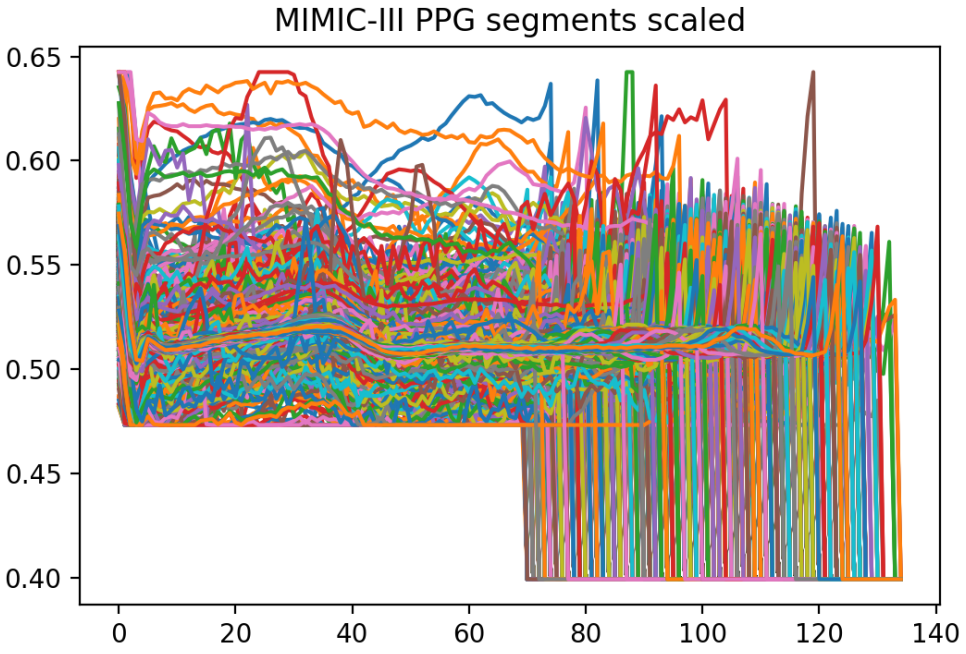

Figure 24 *. Final data for processing after scaling, all data in is between 0 and 1. Values after R-peak are equal to zero.*

The Anomaly detection Framework structure

The Anomaly detection framework is a framework that includes two models which interact with each other in order to achieve higher efficiency and reduce calculation complexity. Full structure of anomaly detection framework is shown in *Figure 25*

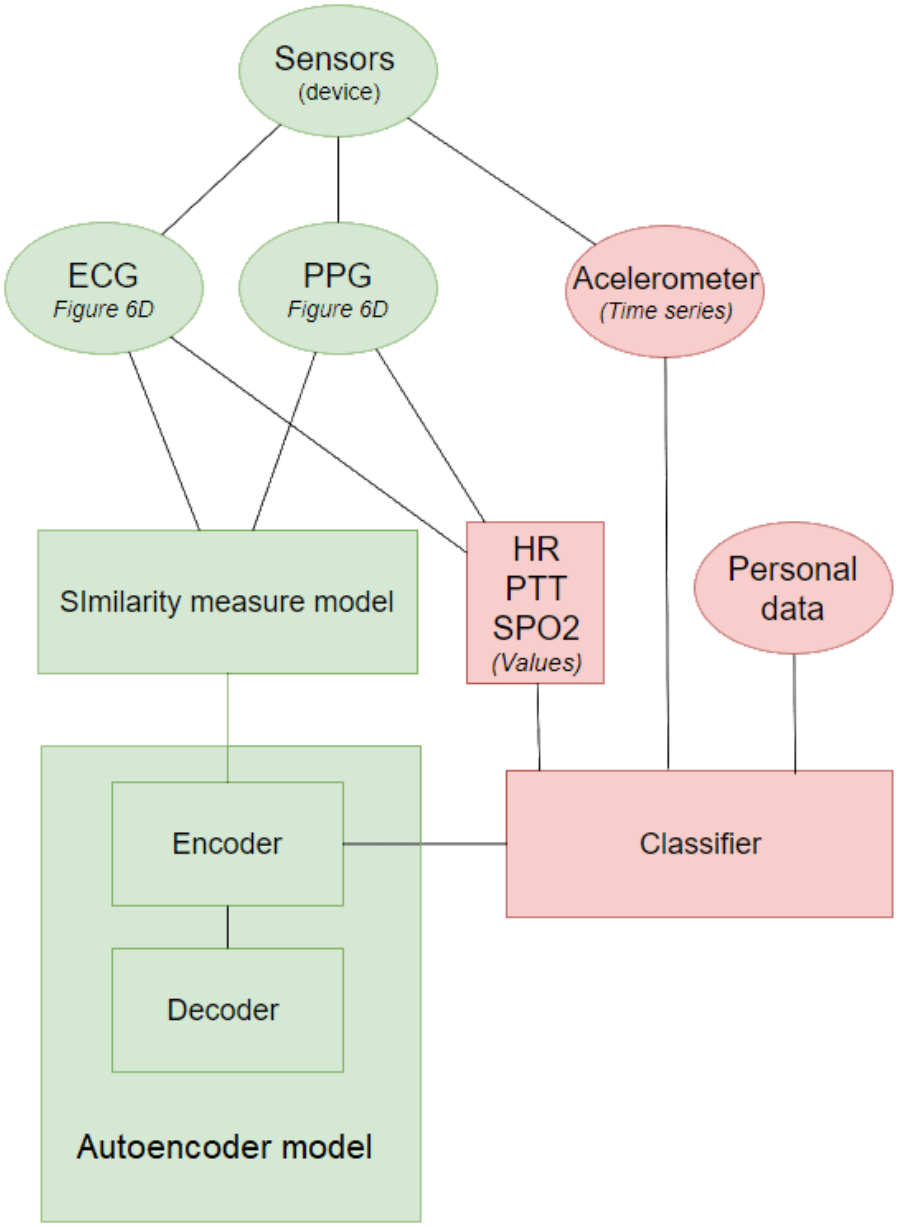

Figure 25. *Scheme of anomaly detection framework. ECG and PPG data goes into the Similarity measure model,then most suspicious data goes to the autoencoder model. Methods that I implement in my work are highlighted with green color, red colors show potential steps.*

Models

The Similarity measure model

There are different advantages and disadvantages of similarity measure approaching in context of my data. To choose between those methods we have to consider variation that occurs in ECG and PPG and calculation complexity. List of available methods is described in section. Similarity measure approach is used as the first stage of anomaly detection, you can see this on scheme (see *Figure 25*).

Dynamic Time Warping demonstrated best results for both ECG and PPG time series segments, because of changes in length of segments, slight change in segment length causes mismatch of time series that leads to increment in similarity measure value. This becomes

even more obvious by looking at data (see Figure 24), normal ECG segments do not change the structure, but they can change length or height.

A similarity measure approach is used for the first stage of my framework. In the first stage we want to detect suspicious segments to use them for further analysis in the more advanced model. My algorithm compares each segment of ECG and PPG with the previous segment of ECG and PPG, this allows to be more flexibility in terms of variation in this time series. My aim is to detect abnormalities in sensor functioning and other suspicious segments which can be classified as symptoms or diseases.

After performing a filtering sample of MIMIC-III data I received similarity measure values that you can see in *Figure 26 (A)*. From this similarity measure distribution I took upper-tail intervals which are equal to 5% and 1% of most suspicious segments. You can see this subsets in *Figure 26 (B,C,D)*.

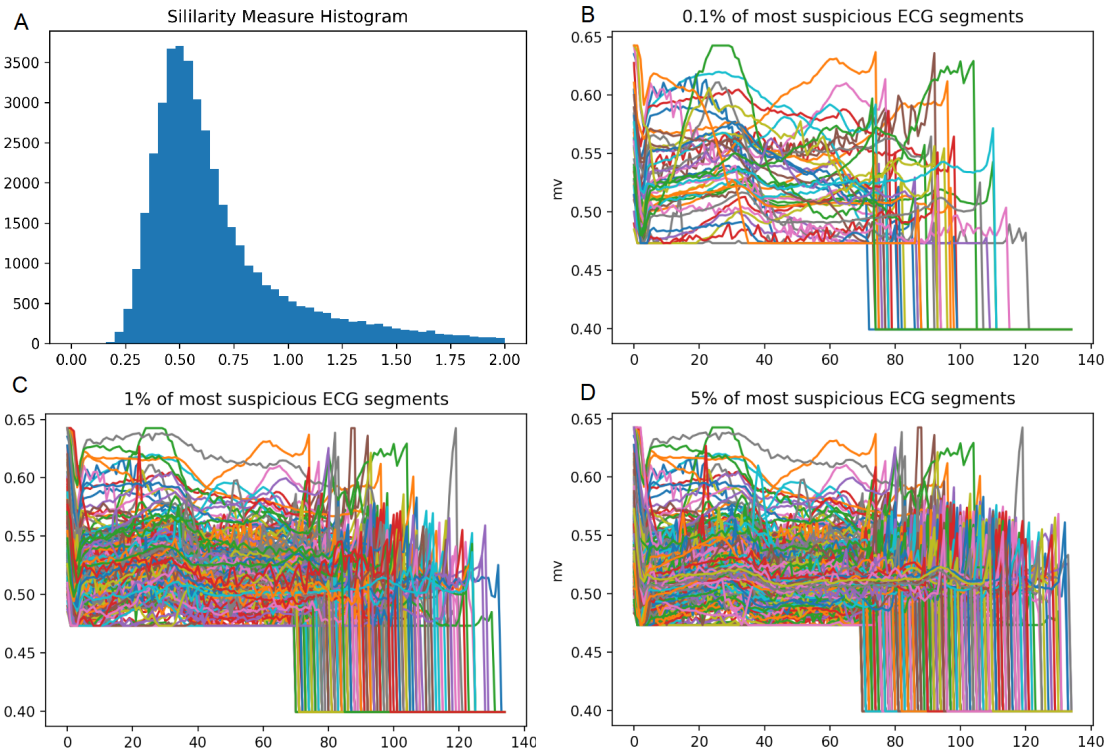

***Figure 26.A**:Histogram of similarity measure values between each ECG segment with his previous ECG segment. Figures **B,C,D** shows sampling of segments with highest similarity measure values with different threshold 0.1%,1%,5%*

Because we compare two neighboring segments ,we can not understand which of throws two elements which one of them is abnormal, that's why we mark them both as suspicious. Further filtering can be done but my aim wes to use this method as preparation. Second limitation is if two abnormal elements are similar and abnormal at the same time they will be detected only once. In result this filtering allowed me to remove 40 000 ECG segments from 42 000 segments what equals to 95%

The Autoencoder model

Convolutional Autoencoder, this type of Autoencoder is proven to be one of the most effective autoencoders for physiological time series anomaly detection[106]. I managed to achieve best result with this type of neural network , compare to Recurrent LSTM autoencoder and Autoencoder based on a fully-connected layer. Convolutional autoencoder showed better results with T and P waves transformation but makes the TP-interval larger with my data. This can be compensated by using dynamic time warping technique for transformation loss calculation.Autoencoder Architecture and code is shown in Appendix 1

The loss function I use for Autoenceder is MSE function (Mean Squared Error) this loos function works better from my case. plot of loss and validation loss is shown in *Figures 27*. For optimizer I choose Adam optimizer[107]. During training process we should look at loss value and validation loss values. As validation data I used thrain data. The figure shows change of loss values by epochs, as we can see after 50 epochs loss and validation loss changes are not significant.

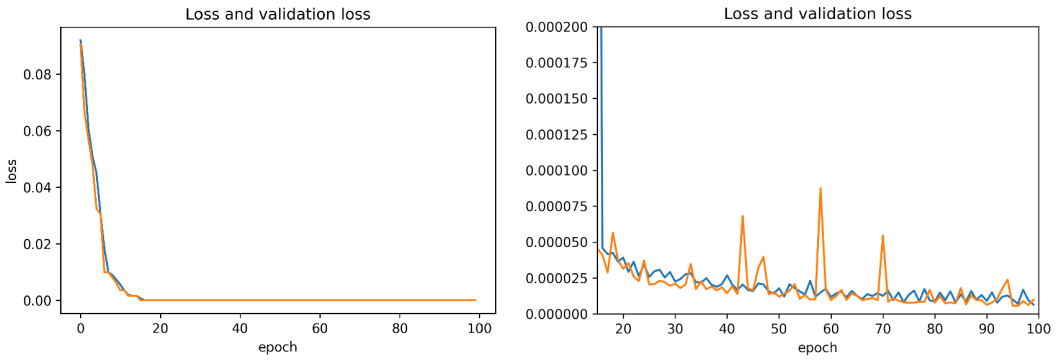

Figure 27*. Loss and validation loss by epoches.Second picture shows same plot but closer in order to inspect overfitting .*

After applying my autoencoder on data from MIMIC-III Waveform matched subsets evaluation data I received next results *Figure 28*. The aim was to receive ECG segments which are close to normal, we can see that it works really good for ECG segments which were lower than others. Our main point of interest were first of all this segments, ECG segments which are higher have worse quality compared to segments which are lower. Changes in filter size did not improve TP-interval transformation, I assume this because of the lack of short ECG segments in training data.

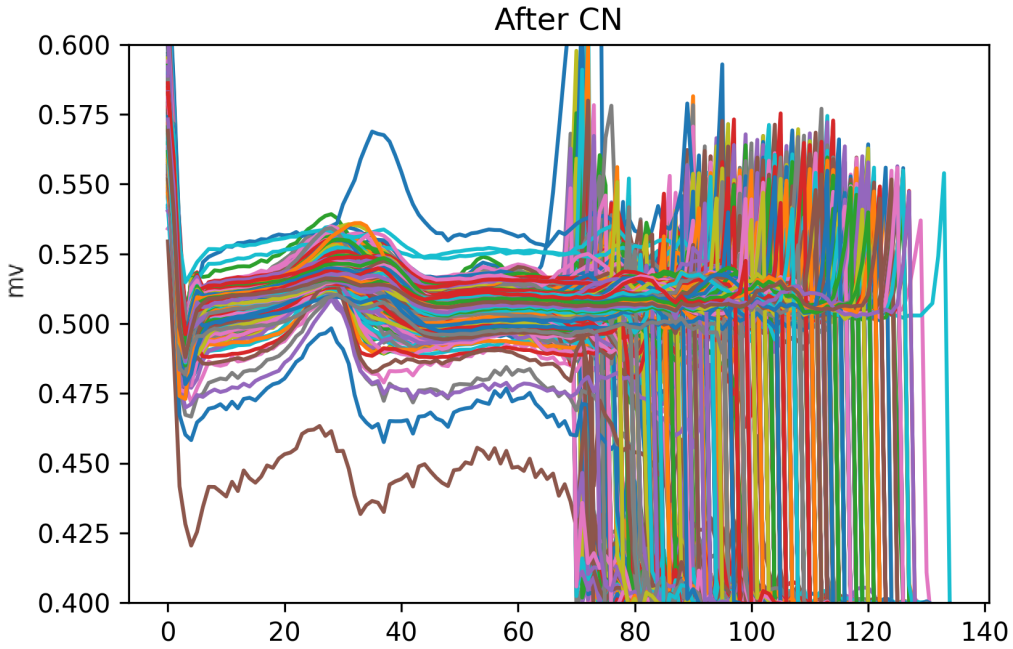

Figure 28. Sample of data after passing through Autoencoder.

After processing all data with Autoencoder we can calculate transformation loss between input(original ECG segments) and output. After calculating transformation loss for each ECG segment we can plot obtained values. You can see a histogram of transformation loss values *Figure 29*, for normal segments transformation loss is low, while for unusual segments transformation loss is high. By looking at histogram we should choose the transformation loss threshold.

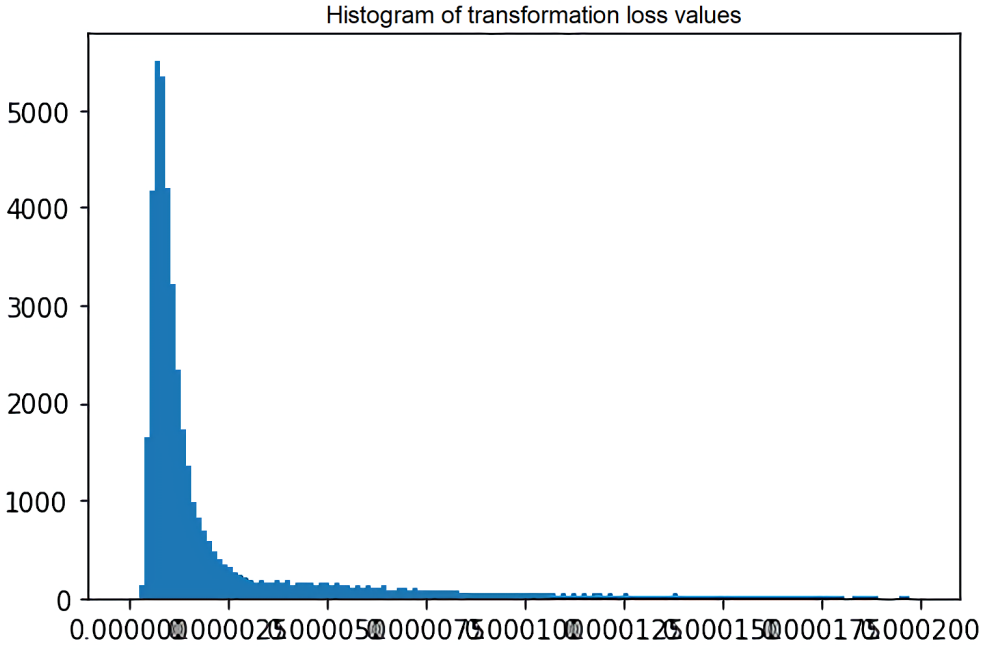

***Figure 29**. Transformation loss values*

After choosing ECG segments above curtain threshold transformation we can consider them abnormal with curtain level of abnormality. For further analysis I took segments with transformation loss higher than 0.0008, in result took 55 segments from 11.6 hours of data. Because high amount of alarms can distract users I took a threshold which is not too low. The threshold can be adjusted for different situations, for clinical application it can be higher for day to day usage like smart-watch application threshold can be higher. *Figure 30* illustrates these segments.

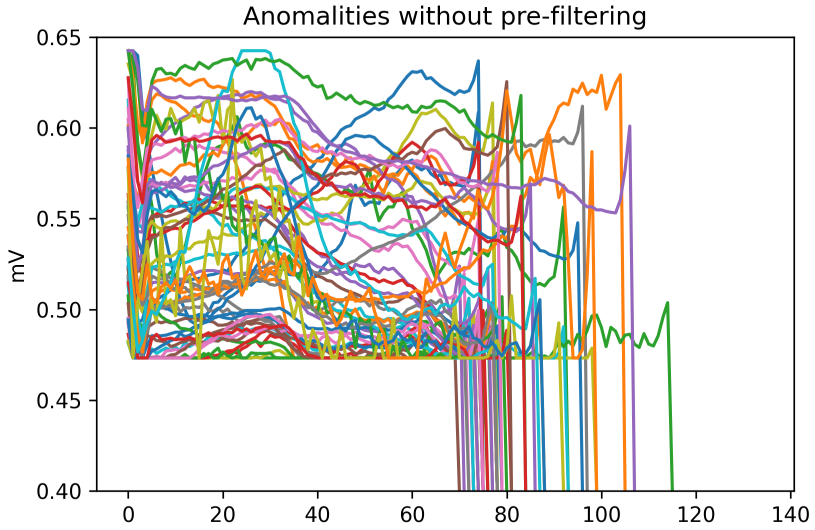

Figure 30. *Segments that autoencoder can detect without pre filtering*

These segments after Autoencoder (see *Figure 31*), we can see most abnormal segments catch different ECG segment patterns(see *FIgure 23*) and transform to the pattern of other patients, which results in high loss.

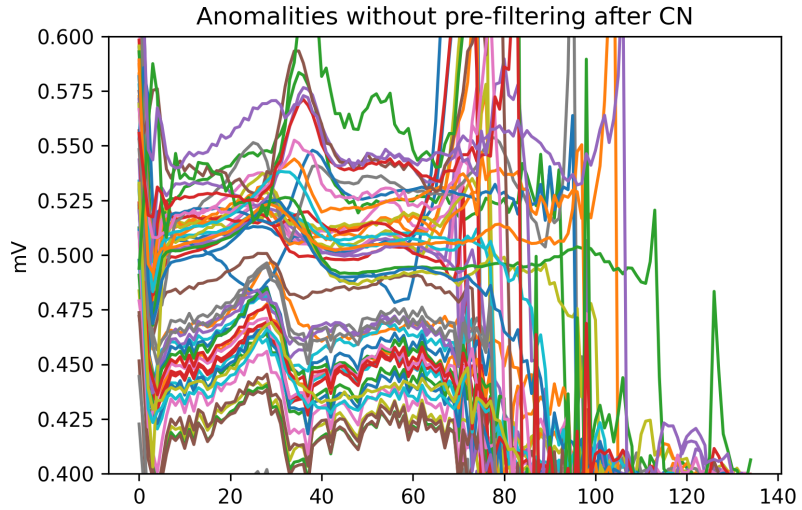

Figure 31. *ECG segments from Figure 35 but after the Autoencoder model transformation*

Anomaly detection framework

My framework uses both methods to combine strong sides of bots algorithms, Similarity measure approach on the first stage is used to filter most obvious normal ECG and more advanced Autoencoder technique is used for more in depth anomaly detection. Similarity measure provides speed and convolutional autoencoder provides wide anomaly detection capabilities. Moreover the whole system is unsupervised and has adjustable thresholds that can regulate the level of abnormality, this makes the system more flexible and allows it to regulate alarms rate.

After performing both methods that have been described above, in a way that is described on scheme(see *Figure 25*), I managed to detect abnormal segments that you can see in Figure 32. Compared to the Autoencoder model without pre-filtering with the Similarity Measure model (see Figure 30) the amount of detected abnormal segments reduced by 20% to 44 segments. These segments are from bottom and have intervals that are similar to T-interval and S-interval, this is happens because the Similarity Measure model considers the streaming nature of data.

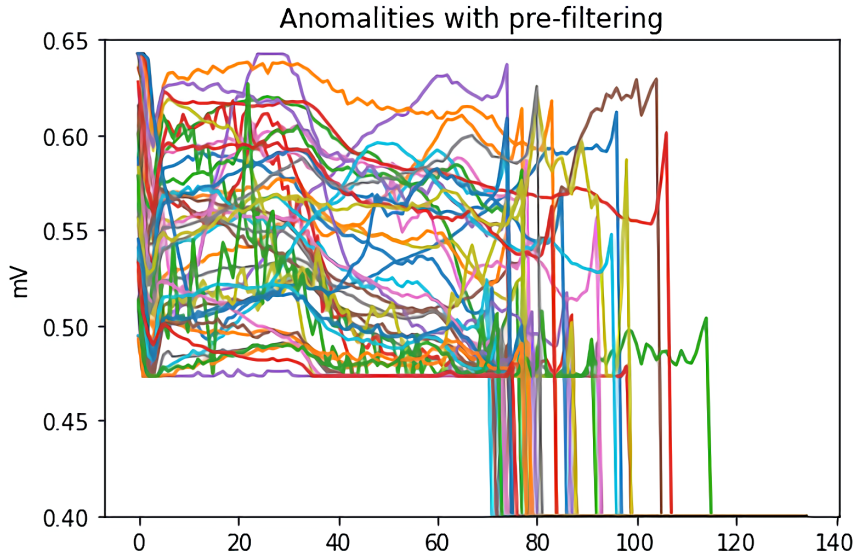

Figure 32 *Abnormal ECG segments after Similarity Measure model and the Autoencoder model.*

A combination of those shows better results in the amount of detected segments over Similarity measure model and advantage in speed over deep learning approach(result can vary depending on hardware). Similarity measure model application provides great possibilities of optimization by including alignment restrictions as mentioned in the description of the algorithm. Alignment restrictions could be adjusted personality for career based on his normal ECG and PPG segmeants. There are more complex autoencoder architectures described in paper [108].

Conclusions

There is an increasing interest in studying various aspects of multidimensional time-series. Especially in recent years, due to the integration of big data technologies, higher usage of sensors, and ability to analyse video data and other signals they are becoming more and more accessible for analysis. The increasing volume of data requires specific tools to be analysed, along with classical data mining techniques similarity measure techniques can be used in detection of anomalies, searching for specific wave forms of time-series. Combination of anomaly detection can significantly save computational resources and increase the effectiveness in both.

This work is focused on the analysis of multivariate time series using a similarity measure in the medical domain. The research presents a framework for multidimensional anomaly detection of anomalies in streaming ECG data. The framework tries to detect anomalies in ECG using PPG as an additional source of information. This solution uses the combination of three components: Data mining to extract cardiac cycle-like segments, Similarity measure model for pre-filtering on extracted segments and Convolutional Autoencoder Model in order to perform more advanced anomaly detection on data that has been received after the previous model. The combination of these techniques allows to increase both detection speed, accuracy and flexibility in terms of regulatable abnormality measure threshold that can be adjusted.

This study is based on an in-depth analysis of current trends and prospective technologies which are already implemented or exist in the early stages of development. The framework was designed with consideration of fundamental constraints of biosensors.

In this research, the author managed to create a robust anomaly detection framework for multidimensional time series. This framework managed to filter 95% (40 000 ECG segments, approximately 8 hours) of data using the Similarity Measure model and pass 5% (2 000 ECG segments) of most suspicious data to the Autoencoder model, which marked 2.2% (44 ECG segments) of received data as abnormal. Similarity Measure model computation complexity is much lower compared to Autoencoder model that includes 1 550 765 parameters. The similarity measure model provides good possibilities for optimization. Performance of the Autoencoder model without pre-filtering with Similarity Measure model amounted to 20% in the amount of detected anomalies.

References

1. Belle, A., Thiagarajan, R., Soroushmehr, S. M., Navidi, F., Beard, D. A., & Najarian, K. (2015). Big data analytics in healthcare. *BioMed research international*, *2015*.
2. Hayward, J., Chansin, G., & Zervos, H. (2016). Wearable Technology 2016–2026 Markets, players and 10-year forecasts. *IDTechEx*.
3. Texas Instruments Wireless ECG, SpO2, PTT and Heart Rate Monitor Reference Design for Medical and Consumer Wearables https://www.ti.com/lit/ug/tidudo6b/tidudo6b.pdf?ts=1622420546890&ref_url=https%253A%252F%252Fwww.ti.com%252Ftool%252FTIDA-01580
4. Moody, B., Moody, G., Villarroel, M., Clifford, G., & Silva, I. (2020). MIMIC-III Waveform Database Matched Subset (version 1.0). PhysioNet. https://doi.org/10.13026/c2294b.
5. García-González, M.A.; Argelagós-Palau, A.; Fernández-Chimeno, M.; Ramos-Castro, J., "A comparison of heartbeat detectors for the seismocardiogram," Computing in Cardiology Conference (CinC), 2013
6. J. Quah "Wearables for Insurance Risk Assessment" https://www.munichre.com/us-life/en/perspectives/wearables/wearables-the-future-is-now-wearables-for-insurance-risk-asses.html
7. H. Han, H. C. Ryoo, and H. Patrick, "An infrastructure of stream data mining, fusion and management for monitored patients," in Proceedings of the 19th IEEE International Symposium on Computer-Based Medical Systems (CBMS '06), pp. 461–468, IEEE, Salt Lake City, Utah, USA, June 2006.
8. N. Bressan, A. James, and C. McGregor, "Trends and opportunities for integrated real time neonatal clinical decision support," in Proceedings of the IEEE-EMBS International Conference on Biomedical and Health Informatics (BHI '12), pp. 687–690, IEEE, Hong Kong, January 2012.
9. D. L. Reich, Monitoring in Anesthesia and Perioperative Care, Cambridge University Press, 2011.
10. M. M. Tisdall and M. Smith, "Multimodal monitoring in traumatic brain injury: current status and future directions," British Journal of Anaesthesia, vol. 99, no. 1, pp. 61–67, 2007.
11. J. C. Hemphill, P. Andrews, and M. de Georgia, "Multimodal monitoring and neurocritical care bioinformatics," Nature Reviews Neurology, vol. 7, no. 8, pp. 451–460, 2011.
12. A. Pantelopoulos and N. G. Bourbakis, "A survey on wearable sensor-based systems for health monitoring and prognosis," IEEE Transactions on Systems, Man and Cybernetics Part C: Applications and Reviews, vol. 40, no. 1, pp. 1–12, 2010.
13. S. Winkler, M. Schieber, S. Lucke et al., "A new telemonitoring ¨ system intended for chronic heart failure patients using mobile telephone technology—feasibility study," International Journal of Cardiology, vol. 153, no. 1, pp. 55–58, 2011.
14. D. Sow, D. S. Turaga, and M. Schmidt, "Mining of sensor data in healthcare: a survey," in Managing and Mining Sensor Data, pp. 459–504, Springer, 2013.
15. Fong, B., Fong, A. C. M., & Li, C. K. (2020). *Telemedicine Technologies: Information Technologies in Medicine and Digital Health*. John Wiley & Sons.
16. Stratifying mortality risk using physical activity as measured by wearable sensor https://www.munichre.com/us-life/en/perspectives/wearables/Stratifying-mortality-risk-using-physical-activity-as-measured-by-wearable-sensors.html
17. Cappuccio, F. P., D'Elia, L., Strazzullo, P., & Miller, M. A. (2010). Sleep duration and all-cause mortality: a systematic review and meta-analysis of prospective studies. *Sleep*, *33*(5), 585-592.
18. Zhang, D., Shen, X., & Qi, X. (2016). Resting heart rate and all-cause and cardiovascular mortality in the general population: a meta-analysis. *Cmaj*, *188*(3), E53-E63.
19. A grassroots initiative by, House Ways & Means Committee ,U.S. Congressman Kevin Brady(2018).50 Ideas to make Healthcare more affordable, accessible and efficient

20. Smith, P. C., & Forgione, D. A. (2007). Global outsourcing of healthcare: a medical tourism decision model. *Journal of Information Technology Case and Application Research*, *9*(3), 19-30.
21. Using Apple Watch for Arrhythmia Detection https://www.apple.com/nz/healthcare/docs/site/Apple_Watch_Arrhythmia_Detection.pdf
22. Mani, A., Rao, S., Nayyar, J., Yan, M., & Johnson, B. (2018). Introduction to the DSP Subsystem in the IWR6843.
23. LeMoyne, R., & Mastroianni, T. (2018). Wearable and Wireless Systems for Healthcare I. *Gait and Reflex Response Quantification*.
24. Han, J., Kamber, M. and Pei, J. 2011. Data Mining: Concepts and Techniques. Elsevier Science.
25. Kurbalija, V. 2009. Time Series Analysis and Prediction Using Case Based Reasoning Technology. University of Novi Sad, Serbia.
26. Radovanović, M. 2010. High-Dimensional Data Representations and Metrics for Machine Learning and Data Mining. University of Novi Sad, Serbia.
27. Agrawal, R., Faloutsos, C. and Swami, A. 1993. Efficient similarity search in sequence databases. Proceedings of the 4th International Conference on Foundations of Data Organization and Algorithms. Springer Berlin Heidelberg. 69–84.
28. Faloutsos, C., Ranganathan, M. and Manolopoulos, Y. 1994. Fast subsequence matching in time-series databases. ACM SIGMOD Record. 23, 2 (Jun. 1994), 419–429.
29. Wu, Y.-L., Agrawal, D. and El Abbadi, A. 2000. A Comparison of DFT and DWT Based Similarity Search in Time-series Databases. Proceedings of the Ninth International Conference on Information and Knowledge Management (New York, NY, USA, 2000), 488–495.
30. Das, G. and Gunopulos, D. 2003. Time Series Similarity and Indexing. The Handbook of Data Mining. N. Ye, ed. Lawrence Erlbaum Associates. 279–304.
31. Goldin, D.Q. and Kanellakis, P.C. 1995. On similarity queries for time-series data: Constraint specification and implementation. Principles and Practice of Constraint Programming — CP ’95 SE - 9. U. Montanari and F. Rossi, eds. Springer Berlin Heidelberg. 137–153.
32. Ratanamahatana, C.A. and Keogh, E. 2005. Three myths about dynamic time warping data mining. Proceedings of SIAM International Conference on Data Mining (SDM’05) (2005), 506– 510.
33. Keogh, E. and Ratanamahatana, C.A. 2005. Exact indexing of dynamic time warping. Knowledge and Information Systems. 7, 3 (May 2005), 358–386.
34. Bouckaert, R. and Frank, E. 2004. Evaluating the Replicability of Significance Tests for Comparing Learning Algorithms. Advances in Knowledge Discovery and Data Mining SE - 3. H. Dai, R. Srikant, and C. Zhang, eds. Springer Berlin Heidelberg. 3–12.
35. Chan, K.-P. and Fu, A.W.-C. 1999. Efficient time series matching by wavelets. Data Engineering, 1999. Proceedings., 15th International Conference on (1999), 126–133.
36. Dudani, S.A. 1976. The Distance-Weighted k-Nearest-Neighbor Rule. Systems, Man and Cybernetics, IEEE Transactions on. 6, 4 (1976), 325–327.
37. Giusti, R. and Batista, G.E.A.. 2013. An Empirical Comparison of Dissimilarity Measures for Time Series Classification. Intelligent Systems (BRACIS), 2013 Brazilian Conference on (Oct. 2013), 82–88.
38. Bala, A., Kumar, A. and Birla, N. 2010. Voice command recognition system based on MFCC and DTW. International Journal of Engineering Science and Technology. 2, 12 (2010), 7335–7342.
39. Górecki, T. and Luczak, M. 2013. Using derivatives in time series classification. Data Mining and Knowledge Discovery. 26, 2 (Mar. 2013), 310–331.
40. Cover, T. and Hart, P. 1967. Nearest neighbor pattern classification. Information Theory, IEEE Transactions on. 13, 1 (1967), 21–27.

41. Dudani, S.A. 1976. The Distance-Weighted k-Nearest-Neighbor Rule. Systems, Man and Cybernetics, IEEE Transactions on. 6, 4 (1976), 325–327.
42. Goldin, D.Q. and Kanellakis, P.C. 1995. On similarity queries for time-series data: Constraint specification and implementation. Principles and Practice of Constraint Programming — CP ’95 SE - 9. U. Montanari and F. Rossi, eds. Springer Berlin Heidelberg. 137–153. 42
43. Yoonseop Kang, Kang-Tae Lee, Jihyun Eun, Sung Eun Park and Seungjin Choi, ‘Stacked Denoising Autoencoders for Face Pose Normalization.’
44. Pascal Vincent, Hugo Larochelle, Isabelle Lajoie, Yoshua Bengio and Pierre-Antoine Manzagol, ‘Stacked Denoising Autoencoders: Learning Useful Representations in a Deep Network with a Local Denoising Criterion.’ (801 citations)
45. Koydemir, H.C.; Ozcan, A. Wearable and Implantable Sensors for Biomedical Applications. Annu. Rev. Anal. Chem. 2018, 11, 127–146.
46. Kapassa, E.; Touloupou, M.; Mavrogiorgou, A.; Kiourtis, A.; Giannouli, D.; Katsigianni, K.; Kyriazis, D. An Innovative EHealth System Powered by 5G Network Slicing. In Proceedings of the 2019 Sixth International Conference on Internet of Things: Systems, Management and Security (IOTSMS), Granada, Spain, 22–25 October 2019; pp. 7–12.
47. Darwish, A.; Hassanien, A.E.; Darwish, A.; Hassanien, A.E. Wearable and Implantable Wireless Sensor Network Solutions for Healthcare Monitoring. Sensors 2011, 11, 5561–5595 47
48. Majumder, S.; Mondal, T.; Deen, M.J. Wearable Sensors for Remote Health Monitoring. Sensors 2017, 17, 130.
49. Darwish, A.; Hassanien, A.E.; Darwish, A.; Hassanien, A.E. Wearable and Implantable Wireless Sensor Network Solutions for Healthcare Monitoring. Sensors 2011, 11, 5561–5595
50. Varatharajan, R.; Manogaran, G.; Priyan, M.K.; Sundarasekar, R. Wearable sensor devices for early detection of Alzheimer disease using dynamic time warping algorithm. Clust. Comput. 2018, 21, 681–690.
51. Parrilla, M.; Guinovart, T.; Ferré, J.; Blondeau, P.; Andrade, F.J. A Wearable Paper-Based Sweat Sensor for Human Perspiration Monitoring. Adv. Healthc. Mater. 2019, 8, 1900342.
52. Cote, G.L.; Lec, R.M.; Pishko, M.V. Emerging biomedical sensing technologies and their applications. IEEE Sens. J. 2003, 3, 251–266.
53. Patel, S.; Park, H.; Bonato, P.; Chan, L.; Rodgers, M. A review of wearable sensors and systems with application in rehabilitation. J. Neuroeng. Rehabil. 2012, 9, 21.
54. Liu, Y.; He, K.; Chen, G.; Leow, W.R.; Chen, X. Nature-Inspired Structural Materials for Flexible Electronic Devices. Chem. Rev. 2017, 117, 12893–12941.
55. Wang, M.; Hu, L.; Xu, C. Recent advances in the design of polymeric microneedles for transdermal drug delivery and biosensing. Lab Chip 2017, 17, 1373–1387.
56. Alexander, H.; Cook, T. Variations With Age In The Mechanical Properties of Human Skin in Vivo. In Bed Sore Biomechanics; Macmillan Education: London, UK, 1976; pp. 109–117
57. . Potts, R.O.; Buras, E.M.; Chrisman, D.A. Changes with Age in the Moisture Content of Human Skin. J. Invest. Dermatol. 1984, 82, 97–100.
58. Daly, C.H.; Odland, G.F. Age-related Changes in the Mechanical Properties of Human Skin. J. Invest. Dermatol. 1979, 73, 84–87.
59. Roudjane, M.; Bellemare-Rousseau, S.; Khalil, M.; Gorgutsa, S.; Miled, A.; Messaddeq, Y.; Roudjane, M.; Bellemare-Rousseau, S.; Khalil, M.; Gorgutsa, S. A Portable Wireless Communication Platform Based on a Multi-Material Fiber Sensor for Real-Time Breath Detection. Sensors 2018, 18, 973.
60. Yamada, T.; Hayamizu, Y.; Yamamoto, Y.; Yomogida, Y.; Izadi-Najafabadi, A.; Futaba, D.N.; Hata, K. A stretchable carbon nanotube strain sensor for human-motion detection. Nat. Nanotechnol. 2011, 6, 296–301.
61. Mathew, J.; Semenova, Y.; Farrell, G. A miniature optical breathing sensor. Biomed. Opt. Express 2012, 3, 3325.

62. Tang, Y.; Zhao, Z.; Hu, H.; Liu, Y.; Wang, X.; Zhou, S.; Qiu, J. Highly Stretchable and Ultrasensitive Strain Sensor Based on Reduced Graphene Oxide Microtubes–Elastomer Composite. ACS Appl. Mater. Interfaces 2015, 7, 27432–27439.
63. Ferrari, M.; Quaresima, V. A brief review on the history of human functional near-infrared spectroscopy (fNIRS) development and fields of application. Neuroimage 2012, 63, 921–935.
64. Lacour, S.P.; Jones, J.; Wagner, S.; Li, T.; Suo, Z. Stretchable Interconnects for Elastic Electronic Surfaces. Proc. IEEE 2005.
65. Park, S.-I.; Ahn, J.-H.; Feng, X.; Wang, S.; Huang, Y.; Rogers, J.A. Theoretical and Experimental Studies of Bending of Inorganic Electronic Materials on Plastic Substrates. Adv. Funct. Mater. 2008. [CrossRef]
66. Li, T.; Huang, Z.Y.; Xi, Z.C.; Lacour, S.P.; Wagner, S.; Suo, Z. Delocalizing strain in a thin metal film on a polymer substrate. Mech. Mater. 2005. [CrossRef]
67. Lu, N.; Lu, C.; Yang, S.; Rogers, J. Highly Sensitive Skin-Mountable Strain Gauges Based Entirely on Elastomers. Adv. Funct. Mater. 2012, 22, 4044–4050.
68. Kim, Y.-C.; Park, J.-H.; Prausnitz, M.R. Microneedles for drug and vaccine delivery. Adv. Drug Deliv. Rev. 2012, 64, 1547–1568.
69. Chang, H.; Zheng, M.; Yu, X.; Than, A.; Seeni, R.Z.; Kang, R.; Tian, J.; Khanh, P.D.; Liu, L.; Chen, P.; et al. A Swellable Microneedle Patch to Rapidly Extract Skin Interstitial Fluid for Timely Metabolic Analysis. Adv. Mater. 2017, 29, 1702243.
70. Mandal, A.; Boopathy, A.V.; Lam, L.K.W.; Moynihan, K.D.; Welch, M.E.; Bennett, N.R.; Turvey, M.E.; Thai, N.; Jenny, V.H.; Love, J.C.; et al. Cell and fluid sampling microneedle patches for monitoring skin-resident immunity. Sci. Transl. Med. 2018, 10.
71. Ribet, F.; Stemme, G.; Roxhed, N. Real-time intradermal continuous glucose monitoring using a minimally invasive microneedle-based system. Biomed. Microdevices 2018, 20, 1–10.
72. Liu, L.; Kai, H.; Nagamine, K.; Ogawa, Y.; Nishizawa, M. Porous polymer microneedles with interconnecting microchannels for rapid fluid transport. RSC Adv. 2016, 6, 48630–48635.
73. Jackson, S.M.; Williams, M.L.; Feingold, K.R.; Elias, P.M. Pathobiology of the stratum corneum. West. J. Med. 1993, 158, 279–285
74. Harding, C.R.; Watkinson, A.; Rawlings, A.V.; Scott, I.R. Dry skin, moisturization and corneodesmolysis. Int. J. Cosmet. Sci. 2000, 22, 21–52.
75. Tobin, D.J. Biochemistry of human skin–our brain on the outside. Chem. Soc. Rev. 2006, 35, 52–67.
76. Kupke, I.R.; Kather, B.; Zeugner, S. On the composition of capillary and venous blood serum. Clin. Chim. Acta 1981, 112, 177–185.
77. Roe, J.N.; Smoller, B.R. Bloodless glucose measurements. Crit. Rev. Ther. Drug Carr. Syst. 1998, 15, 199–241.
78. Aukland, K.; Reed, R.K. Interstitial-lymphatic mechanisms in the control of extracellular fluid volume. Physiol. Rev. 1993, 73, 1–78.
79. Fogh-Andersen, N.; Altura, B.M.; Altura, B.T.; Siggaard-Andersen, O. Composition of interstitial fluid. Clin. Chem. 1995, 41, 1522–1525.
80. Koschinsky, T.; Jungheim, K.; Heinemann, L. Glucose Sensors and the Alternate Site Testing-Like Phenomenon: Relationship Between Rapid Blood Glucose Changes and Glucose Sensor Signals. Diabetes Technol. Ther. 2003, 5, 829–842.
81. Cengiz, E.; Tamborlane, W.V. A tale of two compartments: Interstitial versus blood glucose monitoring. Diabetes Technol. Ther. 2009, 11 (Suppl. 1), S11–S16.
82. Chang, H.; Zheng, M.; Yu, X.; Than, A.; Seeni, R.Z.; Kang, R.; Tian, J.; Khanh, P.D.; Liu, L.; Chen, P.; et al. A Swellable Microneedle Patch to Rapidly Extract Skin Interstitial Fluid for Timely Metabolic Analysis. Adv. Mater. 2017, 29, 1702243.
83. Yang, J.; Liu, X.; Fu, Y.; Song, Y. Recent advances of microneedles for biomedical applications: Drug delivery and beyond. Acta Pharm. Sin. B 2019, 9, 469–483.

84. Yelderman, M.; New, W. Evaluation of Pulse Oximetry. Anesthesiology 1983, 59, 349–351. 84
85. Tremper, K.K. Pulse Oximetry. Chest 1989, 95, 713–715.
86. Elsherif, M.; Hassan, M.U.; Yetisen, A.K.; Butt, H. Wearable Contact Lens Biosensors for Continuous Glucose Monitoring Using Smartphones. ACS Nano 2018, 12, 5452–5462.
87. Wang, D.; Sheng, B.; Peng, L.; Huang, Y.; Ni, Z. Flexible and Optical Fiber Sensors Composited by Graphene and PDMS for Motion Detection. Polymers 2019, 11, 1433.
88. Chen, T.-L.; Lo, Y.-L.; Liao, C.-C.; Phan, Q.-H. Noninvasive measurement of glucose concentration on human fingertip by optical coherence tomography. J. Biomed. Opt. 2018, 23, 1.
89. Guo, J.; Zhou, B.; Zong, R.; Pan, L.; Li, X.; Yu, X.; Yang, C.; Kong, L.; Dai, Q. Stretchable and Highly Sensitive Optical Strain Sensors for Human-Activity Monitoring and Healthcare. ACS Appl. Mater. Interfaces 2019, 11, 33589–33598.
90. Chow, H.-W.; Yang, C.-C. Accuracy of Optical Heart Rate Sensing Technology in Wearable Fitness Trackers for Young and Older Adults (Preprint). JMIR mHealth uHealth 2019, 8, e14707.
91. Millikan, G.A. The Oximeter, an Instrument for Measuring Continuously the Oxygen Saturation of Arterial Blood in Man. Rev. Sci. Instrum. 1942, 13, 434–444
92. Severinghaus, J.W. Takuo Aoyagi: Discovery of Pulse Oximetry. Anesth. Analg. 2007, 105, S1–S4. [CrossRef]
93. Guazzi, A.R.; Villarroel, M.; Jorge, J.; Daly, J.; Frise, M.C.; Robbins, P.A.; Tarassenko, L. Non-contact measurement of oxygen saturation with an RGB camera. Biomed. Opt. Express 2015, 6, 3320–3338.
94. Anderson, R.R.; Parrish, J.A. The optics of human skin. J. Invest. Dermatol. 1981, 77, 13–19. 94
95. de Trafford, J.; Lafferty, K. What does photoplethysmography measure? Med. Biol. Eng. Comput. 1984, 22, 479–480.
96. Vegfors, M.; Lindberg, L.-G.; Öberg, P.Å.; Lennmarken, C. Accuracy of pulse oximetry at various haematocrits and during haemolysis in anin vitro model. Med. Biol. Eng. Comput. 1993, 31, 135–141.
97. Nijboer, J.A.; Dorlas, J.C.; Mahieu, H.F. Photoelectric plethysmography-some fundamental aspects of the reflection and transmission method. Clin. Phys. Physiol. Meas. 1981, 2, 205. 97
98. Ochoa, W.; Ohara, I. The effect of hematocrit on photoelectric plethysmogram. Tohoku, J. Exp. Med. 1980, 132, 413–419.
99. Lindberg, L.G.; Tamura, T.; Öberg, P.Å. Photoplethysmography. Med. Biol. Eng. Comput. 1991, 29, 40–47.
100. Zweifler, A.J.; Trinkaus, P. Occlusive digital artery disease in patients with Raynaud's phenomenon. Am. J. Med. 1984, 77, 995–1001. 1
101. D'Agrosa, L.S.; Hertzman, A.B. Opacity pulse of individual minute arteries. J. Appl. Physiol. 1967, 23, 613–620.
102. Hertzman, A.B.; Randall, W.C. Regional Differences in the Basal and Maximal Rates of Blood Flow in the Skin. J. Appl. Physiol. 1948, 1, 234–241.
103. Johnson, A., Pollard, T., & Mark, R. (2016). MIMIC-III Clinical Database (version 1.4). *PhysioNet*. https://doi.org/10.13026/C2XW26.
104. Moody, B., Moody, G., Villarroel, M., Clifford, G., & Silva, I. (2020). MIMIC-III Waveform Database (version 1.0). *PhysioNet*. https://doi.org/10.13026/c2607m.
105. Makowski, D., Pham, T., Lau, Z.J. *et al.* NeuroKit2: A Python toolbox for neurophysiological signal processing. *Behav Res* (2021). https://doi.org/10.3758/s13428-020-01516-y
106. He, Yangdong, and Jiabao Zhao. "Temporal convolutional networks for anomaly detection in time series." *Journal of Physics: Conference Series*. Vol. 1213. No. 4. IOP Publishing, 2019. 106

107. Kingma, D. P., & Ba, J. (2014). Adam: A method for stochastic optimization. *arXiv preprint arXiv:1412.6980*.
108. Zhang, C., & Chen, Y. (2019). Time series anomaly detection with variational autoencoders. *arXiv preprint arXiv:1907.01702*.
109. Goodfellow, I., Bengio, Y., & Courville, A. (2016). Deep Learning (Adaptive Computation and Machine Learning series).

Appendix 1 (Autoencoder architecture)

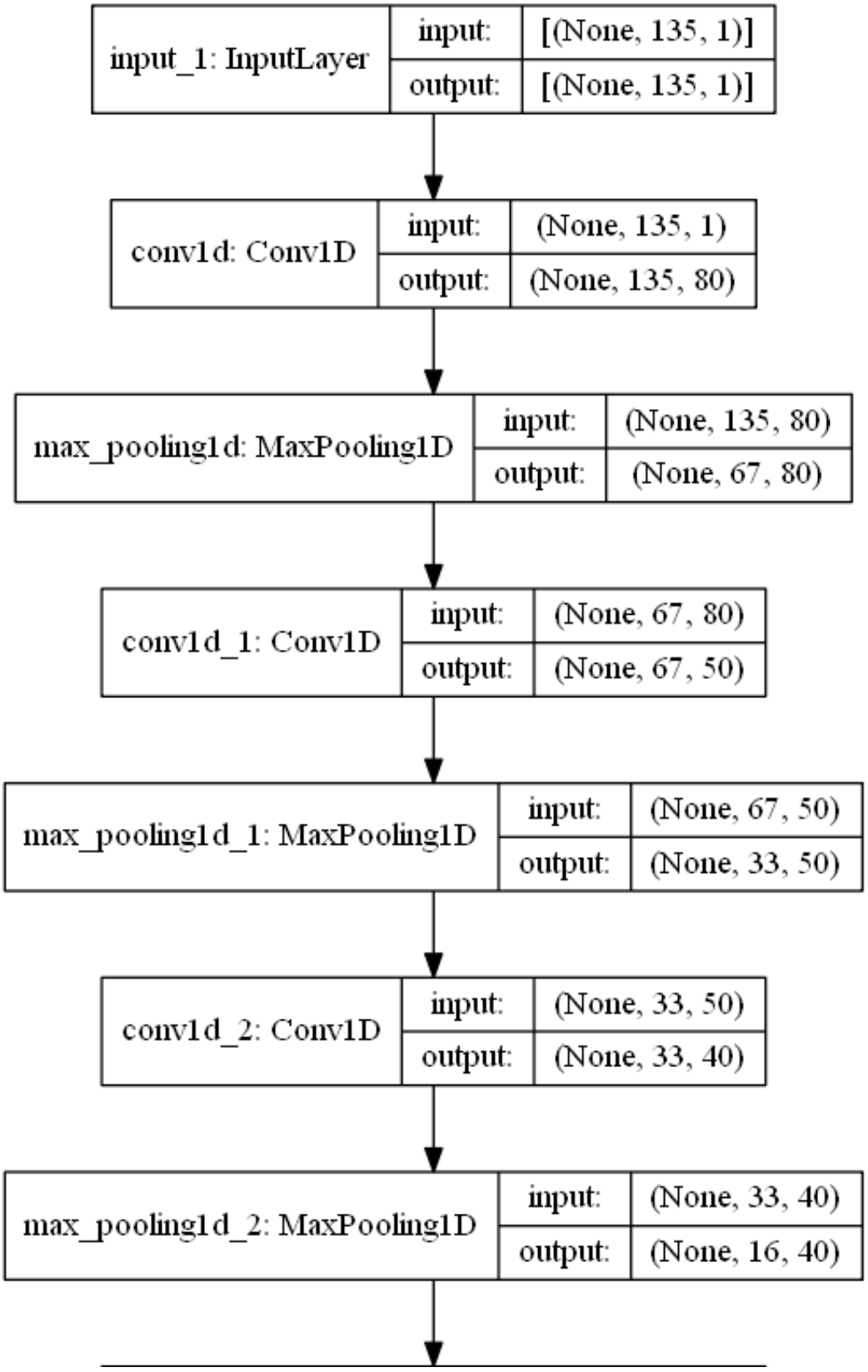

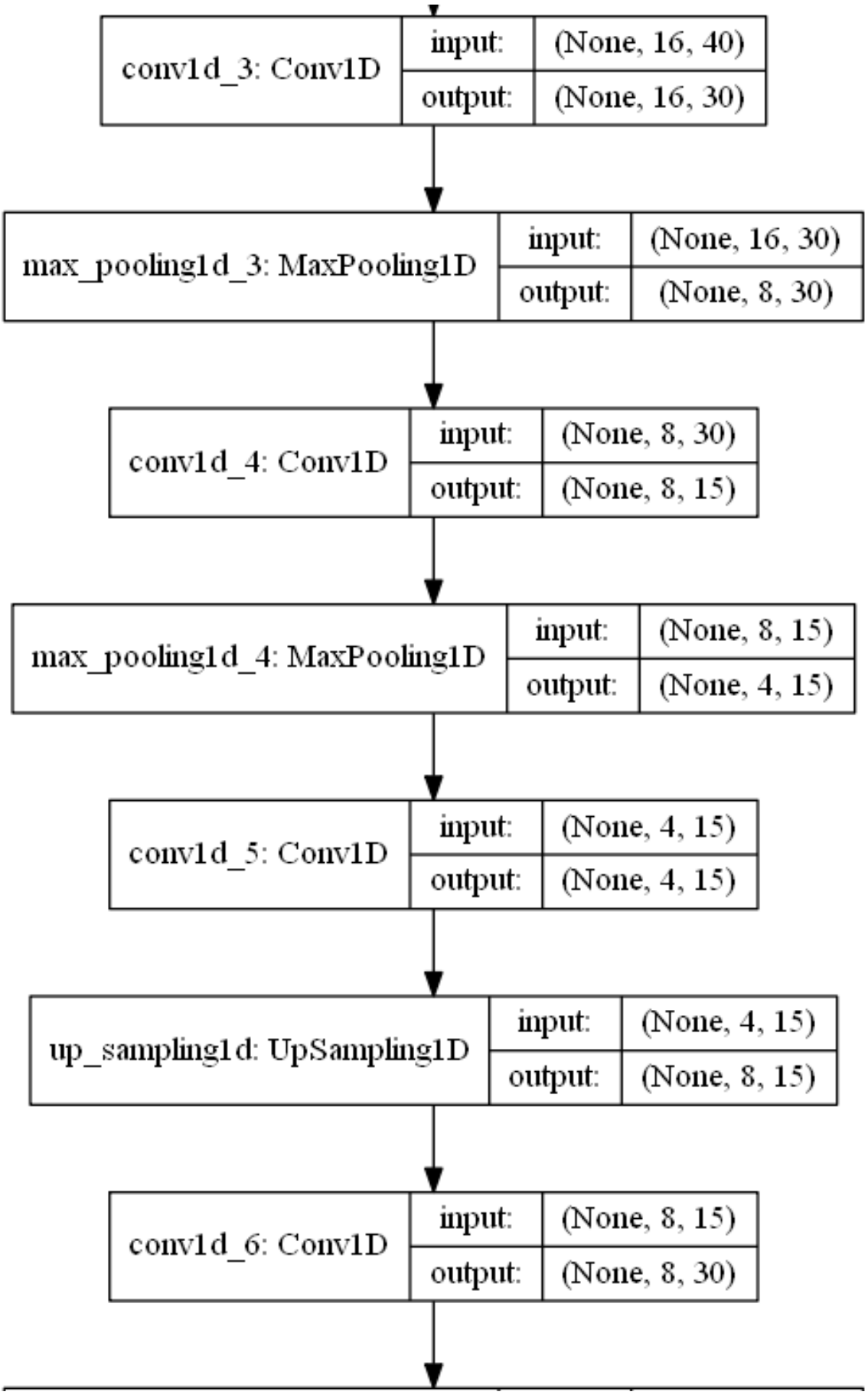
conv1d_3: Conv1D
input: (None, 16, 40)
output: (None, 16, 30)
max_pooling1d_3: MaxPooling1D
input: (None, 16, 30)
output: (None, 8, 30)
conv1d_4: Conv1D
input: (None, 8, 30)
output: (None, 8, 15)
max_pooling1d_4: MaxPooling1D
input: (None, 8, 15)
output: (None, 4, 15)
conv1d_5: Conv1D
input: (None, 4, 15)
output: (None, 4, 15)
up_sampling1d: UpSampling1D
input: (None, 4, 15)
output: (None, 8, 15)
conv1d_6: Conv1D
input: (None, 8, 15)
output: (None, 8, 30)

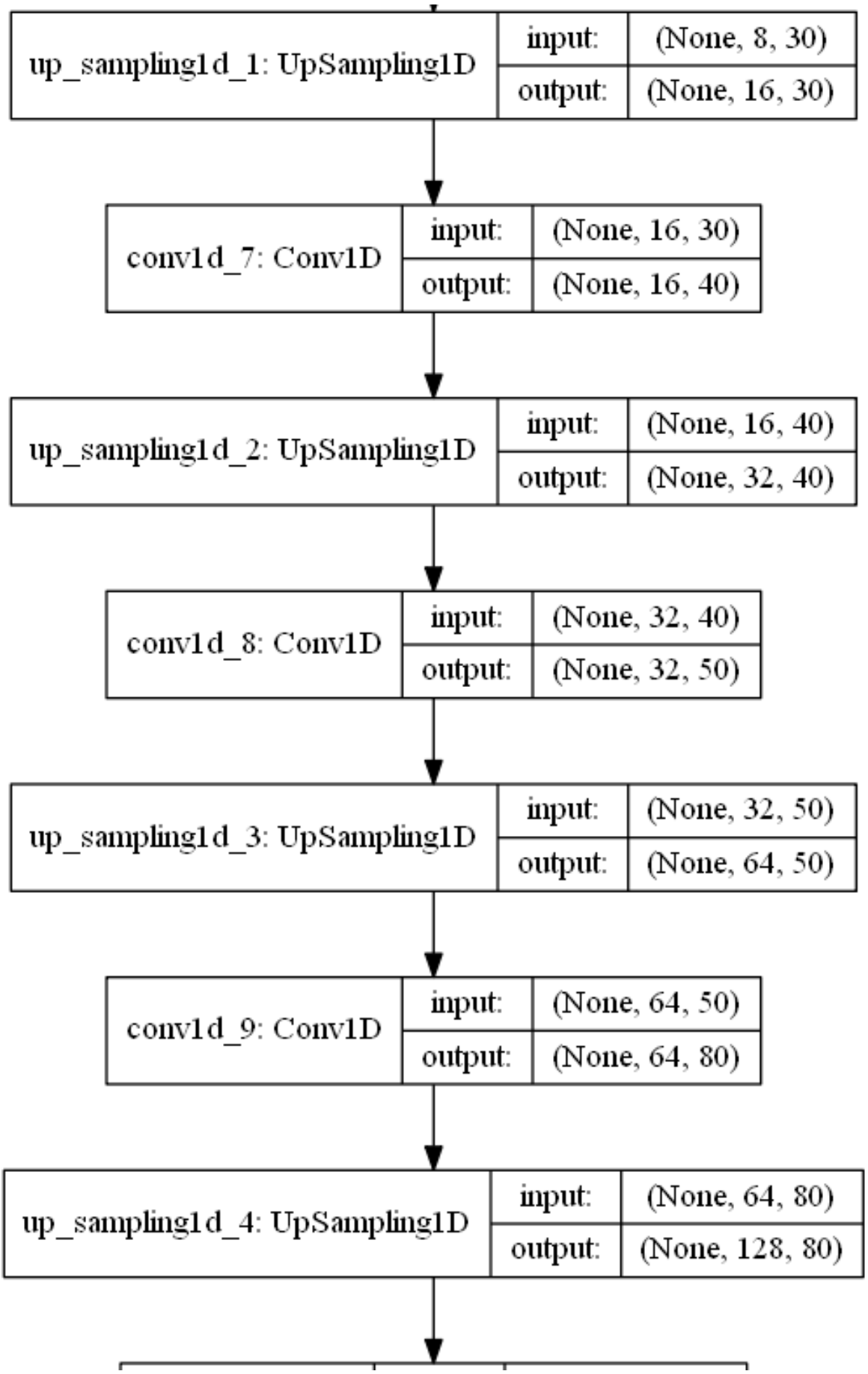
up_sampling1d_1: UpSampling1D
input: (None, 8, 30)
output: (None, 16, 30)
conv1d_7: Conv1D
input: (None, 16, 30)
output: (None, 16, 40)
up_sampling1d_2: UpSampling1D
input: (None, 16, 40)
output: (None, 32, 40)
conv1d_8: Conv1D
input: (None, 32, 40)
output: (None, 32, 50)
up_sampling1d_3: UpSampling1D
input: (None, 32, 50)
output: (None, 64, 50)
conv1d_9: Conv1D
input: (None, 64, 50)
output: (None, 64, 80)
up_sampling1d_4: UpSampling1D
input: (None, 64, 80)
output: (None, 128, 80)

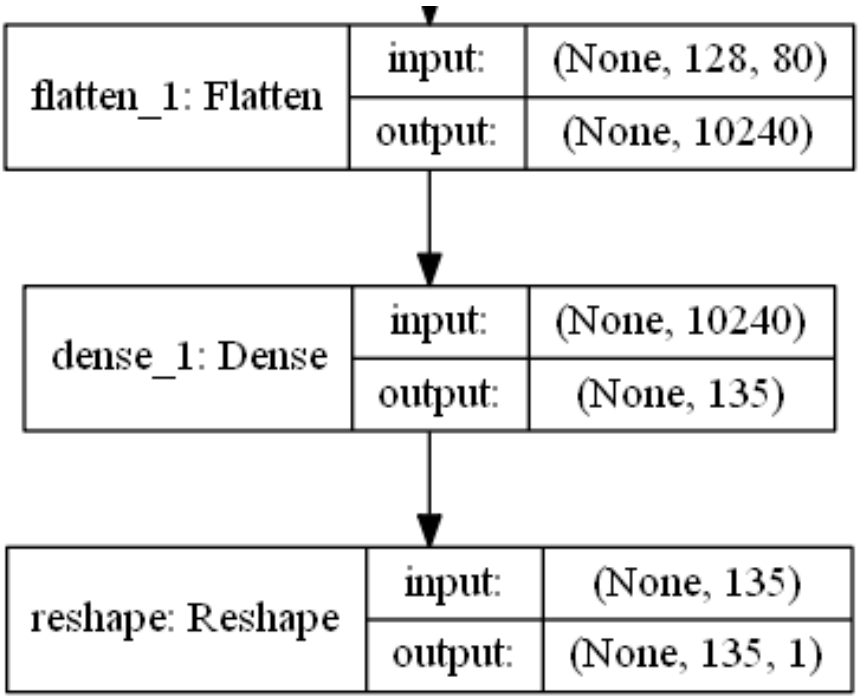

Code :

```
import keras.backend as K
import tensorflow as tf
import keras
from keras.layers import Input, Dense, Conv1D, MaxPooling1D, UpSampling1D, BatchNormalization, LSTM, RepeatVector,Flatten,Reshape
from keras.models import Model

# ENCODER
input_sig = Input(batch_shape=(None,INPUT_LEN,1))
x = Conv1D(80,15, activation='relu', strides= 1,padding=pad, dilation_rate=1)(input_sig )
x = MaxPooling1D(2)(x)
x = Conv1D(50,10, activation='relu',strides= 1, padding=pad, dilation_rate=3)(x)
x = MaxPooling1D(2)(x)
x = Conv1D(40,8, activation='relu', strides=1,padding=pad, dilation_rate=1)(x)
x = MaxPooling1D(2)(x)
x = Conv1D(30,8, activation='relu',strides=1, padding=pad, dilation_rate=2)(x)
x = MaxPooling1D(2)(x)
#x = Conv1D(24,12, activation='relu',strides=strides,padding=pad)(x)
#x = MaxPooling1D(2)(x)
x = Conv1D(15,8, activation='relu', strides=1,padding=pad, dilation_rate=1)(x)
x = MaxPooling1D(2)(x)
flat = Flatten()(x)
encoded = Dense(15,activation = 'relu')(flat)

print("shape of encoded {}".format(K.int_shape(encoded)))

# DECODE
x = Conv1D(15, 8, activation='relu',strides=1, padding=pad, dilation_rate=1)(x)
x = UpSampling1D(2)(x)
#x = Conv1D(24, 6, activation='relu',strides= strides, padding=pad)(x)
#x = UpSampling1D(2)(x)
x = Conv1D(30,8, activation='relu',strides= 1, padding=pad, dilation_rate=2)(x)
```

```
x = UpSampling1D(2)(x)
x = Conv1D(40,10, activation='relu',strides= 1,padding=pad, dilation_rate=1)(x)
x = UpSampling1D(2)(x)
x = Conv1D(50,10, activation='relu',strides= 1, padding=pad, dilation_rate=3)(x)
x = UpSampling1D(2)(x)
x = Conv1D(80, 15, activation='relu',strides=1, padding=pad, dilation_rate=1)(x)
upsamp = UpSampling1D(2)(x)
flat = Flatten()(upsamp)
decoded = Dense(INPUT_LEN,activation = 'relu')(flat)
decoded = Reshape((INPUT_LEN,1))(decoded)

print("shape of decoded {}".format(K.int_shape(decoded)))

#compile model

autoencoder = Model(input_sig, decoded)
autoencoder.compile(optimizer='adam', loss= 'mse' )
```